Nano Today (2012) 7, 430—447

Available online at www.sciencedirect.com

SciVerse ScienceDirect

journal homepage: www.elsevier.com/locate/nanotoday

REVIEW

Graphene-based multilayers: Critical evaluation of materials assembly techniques

Ming Yang[a,1], **Ying Hou**[d,1], **Nicholas A. Kotov**[a,b,c,*]

[a] *Department of Chemical Engineering, University of Michigan, Ann Arbor, MI 48109-2136, United States*
[b] *Department of Materials Science and Engineering, University of Michigan, Ann Arbor, MI 48109-2136, United States*
[c] *Department of Biomedical Engineering, University of Michigan, Ann Arbor, MI 48109-2136, United States*
[d] *Nico Technologies, Green Road, P.O. Box 131221, Ann Arbor, MI 48113, United States*

Received 1 June 2012; received in revised form 1 August 2012; accepted 17 August 2012
Available online 30 September 2012

KEYWORDS
Layer-by-layer (LBL);
Graphene;
Vacuum assisted flocculation (VAF);
Nanosheets;
Multilayers;
Composites

Summary Utilization of unique properties of nanoscale graphene in macroscale materials requires a thoughtful selection of processing method(s). Here we review different materials assembly techniques which result in layered composite reminiscent of many biomaterials with the focus on layer-by-layer (LBL) assembly, vacuum-assisted flocculation (VAF), and others. Critical evaluation of LBL and its comparison to other solution-based methods of materials assembly using the abundant experimental data with graphene and graphene oxide is the main essence of this review. We compare several fundamental characteristics and applications being discussed for graphene-based material such as transparent conducting films, field effect transistors, lithium ion batteries, supercapacitors, solar cells, sensors and polymer nanocomposites, highlighting the strengths, the weaknesses, and expected points of further developments of different techniques. The principle goal to be achieved in the future is to define much better effective implementation of layer-by-layer assembly and other techniques resulting in layered composites taking into account potential technological areas of applications.

Introduction

Modern nanotechnology has become integral to the material sciences, covering all aspects of preparation, fabrication, and application. The advances in synthesis technique, largely enrich the spectrum of nanoscale materials, including two-dimensional (2D) nanosheets, which represent a diverse and unique research target with exciting results based on the existence of single-layer graphene nanosheets composed of carbon atoms arranged in tightly bound hexagons just one atom thick (Fig. 1a). Similar to other nanostructures exhibiting size- and shape-dependent characteristics, graphene shows different properties when compared with its 1D allotrope, i.e. carbon nanotubes (CNTs). The 2D structure of graphene makes it more compatible with planar substrates than typical random distribution of CNTs, making graphene a viable replacement of silicon.

* Corresponding author at: Department of Chemical Engineering, University of Michigan, Ann Arbor, MI 48109-2136, United States.
E-mail address: kotov@umich.edu (N.A. Kotov).
[1] These two authors contributed equally to this work.

1748-0132/$ — see front matter © 2012 Elsevier Ltd. All rights reserved.
http://dx.doi.org/10.1016/j.nantod.2012.08.006

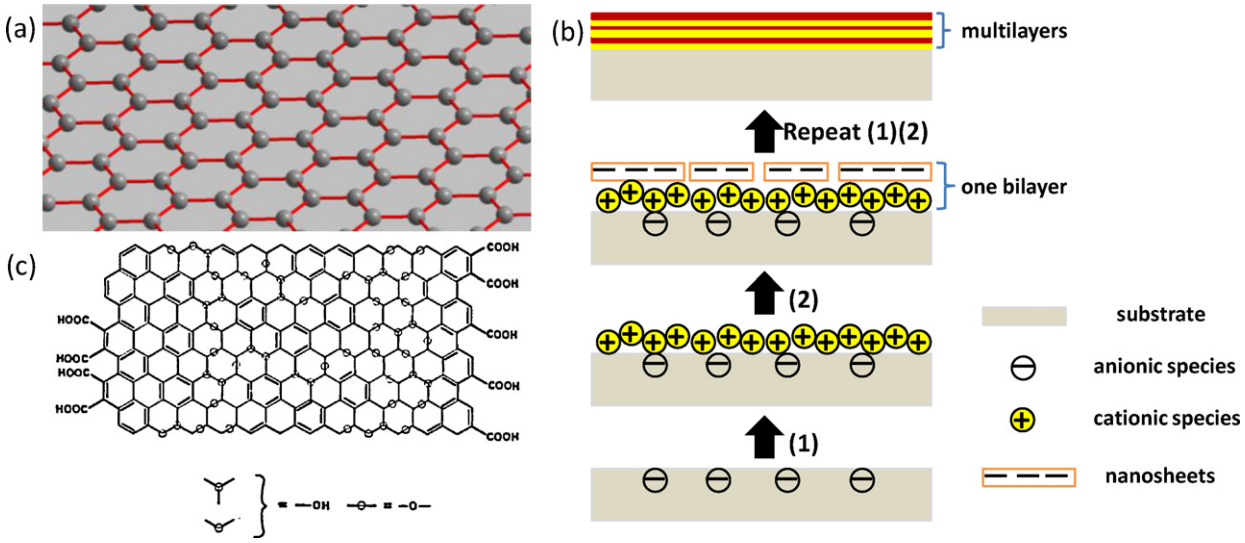

Figure 1 (a) Crystal structure of graphene. (b) Schematic illustration of LBL assembly with negatively charged nanosheets. (c) Chemical structure of graphene oxide.
Reprinted from Ref. [21] with permission by American Chemical Society.

The 2D structures of graphene nanosheets and their atomic scale thickness impart them with unusual properties. The confinement of electrons, anisotropic transportation, and high surface-to-volume ratio are the most stimulating characteristics of the unique sheet-like structures. Intrinsic graphene is a zero-gap semiconductor with remarkably high electron mobility at room temperature (in excess of $15{,}000\,cm^2\,V^{-1}\,s^{-1}$ [1]). The resistivity of graphene ($10^{-6}\,\Omega\,cm$) is lower than that of silver [2]. Individual platelets of graphene also appear to be one of the strongest materials ever tested with a breaking strength 200 times greater than steel and a tensile strength of 130 GPa. They are very stiff, too, and the Young's modulus of graphene is about 1 TPa [3]. Notably, the extraordinary properties cited are only observed in the nearly perfect structure of mechanically exfoliated graphene from highly oriented pyrolitic graphite. The tedious process and low yield necessitates other methods for easy production of graphene with comparable properties. CVD [4] and epitaxial growth [5] of graphene on specific substrates are good alternatives, however, high temperature processing is needed.

Apart from the above-mentioned methods, the solution-based production of graphene receives a lot of attention. With inexpensive sources and high yield production, solution-based method produces stable dispersions that can be used for the easy fabrication of thin film composites. It is necessary to point out that graphene from this method usually bears chemical moieties that on one hand, could degrade the electronic structure of graphene, but could also provide a way to modify the properties of graphene. Currently there are two main methods used to obtain solution processed graphene (SPG). One method consists of dispersing graphite in a proper liquid medium (mostly N-methylpyrrolidone (NMP)) that is then sonicated followed by the separation of non-exfoliated graphite from graphene by centrifugation [6]. The other method utilizes graphene oxide (GO) as a precursor and is probably the most efficient way to produce a large amount of SPG. Graphite is first treated with a strong oxidation agent (a mixture of sulfuric acid, sodium nitrate, and potassium permanganate) to produce GO [7], which typically preserves the layer structure of the parent graphite with the generated oxygen moieties. GO disperses readily in water thanks to the hydrophilic nature of surface functionalities, breaking up into macroscopic flakes, mostly one layer thick. Chemical reduction of GO dispersion would yield a suspension of reduced GO (rGO) stabilized by added polymers [8] or surface charges under certain pH environment [9]. However, as expected, the chemical treatment brings many unavoidable defects, which are typically incompletely removed by existing reduction methods [10].

There are several methods for the manufacture of SPG into thin film composites. Layer-by-layer (LBL) assembly was probably used first [11], followed by vacuum assisted flocculation (VAF) [12] and spin-coating [13] among the most popular, resulting in the films with micron-scale thickness and reasonably high uniformity. Other methods include spray-coating [14], Langmuir—Blodgett (LB) assembly [15], dip-coating [16] and solution blending [17]. One of the challenges in the solution-based methods is retaining the few-layer nature of SPG. SPG's tendency to aggregate usually presents a problem due to the attraction between individual layers; dilute dispersions of SPG are strongly preferred. Furthermore, most of the mentioned solution-based methods control the structure of thin film composites by adjusting the concentration of SPG dispersions, which does not necessarily guarantee a nanoscale uniformity of composites for methods involving direct mixing with a possibility for phase separation. Nanoscale uniformity (or, at least control, over nanoscale heterogeneity) is critically important for properties of composite and other materials.

Biomimetic strategy to produce the hierarchical organization with nanometer precision could be beneficial, because the intriguing layered structure of teeth, bone and nacre consisting of soft proteins and hard minerals gives them remarkable properties. The replication of nacre's brick-and-mortar arrangement is made possible by the 2D

structure of SPG and would provide an elegant way to prepare high performance materials. Moreover, the excellent electrical conductivity of graphene and SPG would be another benefit, especially when compared with clay nanosheets. To this end, LBL, VAF as well as other techniques would be a good choice in the preparation of biomimetic layered SPG multilayers, allowing molecular to nanoscale level control of the material structure. However, there is currently no review discussing the relative advantages of the SPG-based materials made by these techniques. The success in the preparation of clay and CNTs composites [18] promotes us to explore the potential of using LBL assembly to improve the performance of SPG based nanostructures and understand better the challenges related to structural control in this area. Here we review the layered assemblies of SPG with probably somewhat greater focus on LBL assembly due to greater experience in this area; particular attention will be given to the performance comparison of composites made by LBL and different other methods. The challenges and further options in this field are discussed.

LBL assembly

Concept of LBL assembly

The idea of LBL assembly is based on the sequential adsorption of different macromolecular components exhibiting attractive forces between them. The attractive interactions may include electrostatic interactions, hydrogen bonding, van der Waals forces, electron exchange, and a number of others. The general concept of LBL assembly makes this method very effective in the combinations of different kinds of materials (CNTs, clays, nanoparticles (NPs), polymers, proteins, etc.). Typically, substrates are immersed into two different solutions containing target materials alternatively for certain time, with intermittent rinsing and drying steps. The rinsing steps are tremendously important in materials performance because they remove excess of both components adsorbed in disordered form and leave behind the components strongly adhering to the previous layer. Cyclic repetition of the adsorption processes results in the multilayered and ordered structures (Fig. 1b). For more inclusive information about LBL assembly, readers can refer to our previous reviews [18,19] and the book edited by Decher and Schlenoff [20].

Structure of SPG related to LBL assembly

One of the differences between SPG and pure graphene is the presence of oxygen in SPG, mostly in the form of hydroxyl and epoxy groups on the basal plane and smaller amount of carboxyl and carbonyl groups primarily at the sheet edges [21] (Fig. 1c). Because the oxygen is involved during the oxidation, different degrees of oxidation will give different C:O ratio and the amount of functional groups can be altered [22]. The stability of GO dispersion is attributed to the electrostatic repulsion between charged functional groups with a negative surface potential. The presence of functional groups provides the opportunity of introducing GO into LBL assembly by potential hydrogen bonding and electrostatic interactions. After reduction, the amount of oxygen is largely decreased with a partial restoration of sp^2 conjugated carbon atoms [23]. Complete removal of oxygen is usually hard to achieve [9], and the residual groups containing oxygen can be used as attractive sites for other components during LBL assembly. The presence of oxygen functional groups also facilitates further chemical modifications to enhance the stability of SPG in different solvents and improve the interactions between SPG and polymers. For more information about chemical modifications of SPG, readers can refer to the review by Ruoff's group [24]. We also want to point out that the attractions between basal planes of SPG due to van der Waals forces and $\pi-\pi$ stacking could also contribute to the stability of LBL assembled multilayers.

The presence of multiple functional groups on the surface of GO platelets and sp^3 carbon atoms result in the increase of the sheet thickness to ca. 1 nm [25] compared with ca. 0.34 nm seen in mechanically exfoliated graphene [1]. The thickness of rGO with smaller percentage of oxygen is intermediate between GO and graphene. It is noted that the atomically rough and disordered GO still preserve the honeycomb lattice of graphene [21]. However, the roughness of LBL layer of GO is typically much higher than that of individual GO sheets, because (1) nanosheets are adsorbed as stacks due to the short-range attraction forces augmented by the presence of the polymer as LBL partner; (2) the folding of nanosheets may occur during the LBL assembly; (3) intrinsic roughness of the polymer layer adsorbed to the substrate could be high as well.

The lateral dimensions of GO are usually widely distributed ranging from less than 100 nm to several mm and could be roughly controlled by oxidation [22] or ultrasonication [26]. The wide distribution of lateral sizes could be another reason for the reduced ordering of the SPG multilayers. Larger SPG nanosheets can cover wider area without exposing the underlying polymer layer, while smaller ones have to form stacks to get similar results. Consequently, the difference in the size of individual nanosheets may translate into a thickness variation of the SPG layer. In addition, one might anticipate that larger nanosheets would reduce interlayer mixing and promote ordering in the multilayers by covering defects in polymer layers. However, the presence of larger SPG nanosheets will also improve the possibility of forming stacks in the solution due to the stronger van der Waals forces provided. Overall, relatively uniform-sized SPG would be expected to form more ordered multilayers.

The discussed structural characteristics of SPG could lead to the greater than unity number of nanosheets in the SPG multilayers. The interlayer spacing is therefore larger than the sum of the thickness of the polymer layer and monolayer SPG. Larger interlayer spacing is expected for GO based multilayers compared with that of rGO, due to the presence of multiple functional groups, which not only increase the thickness of the platelets, but also promote the adsorption of the polymer layer. A constant interlayer spacing is the basis for the linear growth of the film, which correlates with the high ordering of the multilayers. The study of the thermodynamic and kinetic assembly of SPG and polymer is important for the better control over interlayer spacing, which will determine the accessibility of SPG by foreign materials. The accommodation of substances into the

multilayers with size selectivity is possible by adjusting the interlayer spacing.

The reduction of GO is usually a necessary process to regain the electronic structure of graphene. In LBL assembly, this could be done either before or after the formation of multilayers. A post annealing process is usually applied to further the restoration of the conjugated structure. One may believe that the post-reduction of GO-based assemblies will weaken the multilayers, because the reduction eliminates surface charges when GO is converted into rGO. However, the reduction of the interlayer spacing and the restoration of the conjugated structure during the post-reduction, could support the stability of the multilayers by strengthening the van der Waals interactions and $\pi-\pi$ stacking. A balance needs to be set up between the stability of the film and the restoration of the sp^2 conjugation of graphene.

LBL assembly of SPG

LBL assembly of GO

Although the first synthesis of GO dates back to Brodie's work in 1859 [27], it was not until 1996 that the first layered assemblies of graphene and GO were demonstrated in the early work of Kotov et al. [11] before the discovery of the unique electrical properties of individual sheets of graphene [28]. The use of hydrophilic GO avoids the dispersion problem of graphite making not only the preparation of GO thin film possible but also providing a practical way to reconstruct the structure of graphite useful for a variety of applications. Positively charged poly(diallyldimethylammonium chloride) (PDDA) was selected as the partner polymer of negatively charged GO to facilitate the electrostatic attraction. Self-assembly of the successive PDDA/GO layers was monitored by absorption spectrophotometry showing good linearity. The average thickness of the PDDA layer and GO layer was estimated to be 16 ± 3 Å and 22 ± 5 Å, respectively, based on surface plasmon (SP) spectroscopy. The AFM measurement further revealed the height of each GO layer to be between 18 Å and 28 Å in the self-assembled film. These results indicated that the self-assembled film is composed of 2—3 GO nanosheets in each bilayer considering the basal spacing of GO sheets to be 7.37 Å. Interestingly, this behavior is quite similar to that observed for the self-assembled PDDA/clay thin film [29], implying the comparable absorption characteristic between clay and GO nanosheets. In summary, this work proves the feasibility of using LBL assembly to prepare ultrathin functional GO hierarchical film.

A more detailed study by Kovtyukhova et al. used natural graphite to prepare colloids of GO. This resulted in the production of much larger GO nanosheets with lateral dimensions up to 9 μm [30]. It was also found that the thickness of the GO nanosheets to be smaller than those used by Kotov et al. [11] which they attributed to the use of a more diluted solution. These differences may deserve more attention during the preparation and use of GO dispersion. Linear growth of various polymers and GO was similarly observed. Interestingly, the thickness increment of multilayered GO/poly(allylamine hydrochloride) (PAH) film was found to be 2—3 times the monolayer thickness, which can be partially attributed to the folding of the GO layer (Fig. 2a). The multilayer adsorption model proposed by Kleinfeld and Ferguson for clay/polycation films may also be responsible for the growth of GO/PAH film [31]. It was also found that larger sheets could cover an area which exceeds the area of voids between the sheets and yield the most compact and smooth film. This behavior is also similar with the growth of clay film [32].

Another important factor that needs to be carefully studied besides the influence of graphite source and the concentration of GO dispersion is the degree of oxidation of GO. This will not only affect the surface properties of GO nanosheets, but also have great impact on the quality of the sheets and the state of defects. Cassagneau et al. synthesized GO with different degrees of oxidation and found that oxidative treatment had a significant effect on the thickness of the nanoplatelets, which diminished with the extent of the oxidation [22]. Furthermore, the titration of the GO dispersions indicated that the number of exchangeable protons and the charge density decreased with the extent of oxidation. This observation implied that the carboxyl groups became more labile upon further oxidation and more nonexchangeable hydrogen atoms were incorporated into GO in the form of C—OH. The element analysis of the GO prepared by the adapted Brodie's method [27] used in this work showed that such a method did not lead to the ideal graphitic oxide compound $C_8O_2(OH)_2$ as reported by Touzain et al. [33] and the oxidation extent was lower than that obtained by using H_2SO_4 [7]. These results further emphasize the importance of the preparation procedure in determining the properties of GO nanosheets. However, no correlation between oxidation extent of GO and the properties of multilayers was investigated.

Recently, selective modification of patterned templates with 11-amino-1-undecanethiol (AUT) were used to precisely locate where the electrostatic interactions can take place on GO nanosheets [34] (Fig. 1a—e). The assembly could be turned on and off by adjusting the pH of the solution showing the flexibility of self-assembly based on electrostatics.

LBL assembly of rGO

The recent availability of the stable rGO dispersions fueled enthusiasm for preparation of rGO based multilayered structures without the additional post reduction process to convert GO into rGO in the thin film state [11]. One example is to use rGO stabilized by the carboxylic groups on the edge to assemble with PDDA [9]. The stepwise increase of rGO absorption around 270 nm signified the successful assembly (Fig. 2b). Other methods to stabilize rGO rely on the introduction of extraneous polymers. The polymer stabilized rGO can be achieved by either covalent or noncovalent chemical modifications, both of which improve the stability of rGO via repulsion between polymers. For example, Shen et al. used radical polymerization to prepare negatively charged poly(acrylic acid) (PAA) functionalized rGO and positively charged poly(acryl amide) (PAM) functionalized rGO, respectively [35]. These functionalized rGO can be directly used for the construction of rGO multilayers. Alternatively, Liu et al. fabricated multilayered film by using pyrene-terminated poly(2-N,N′-(dimethyl amino ethyl

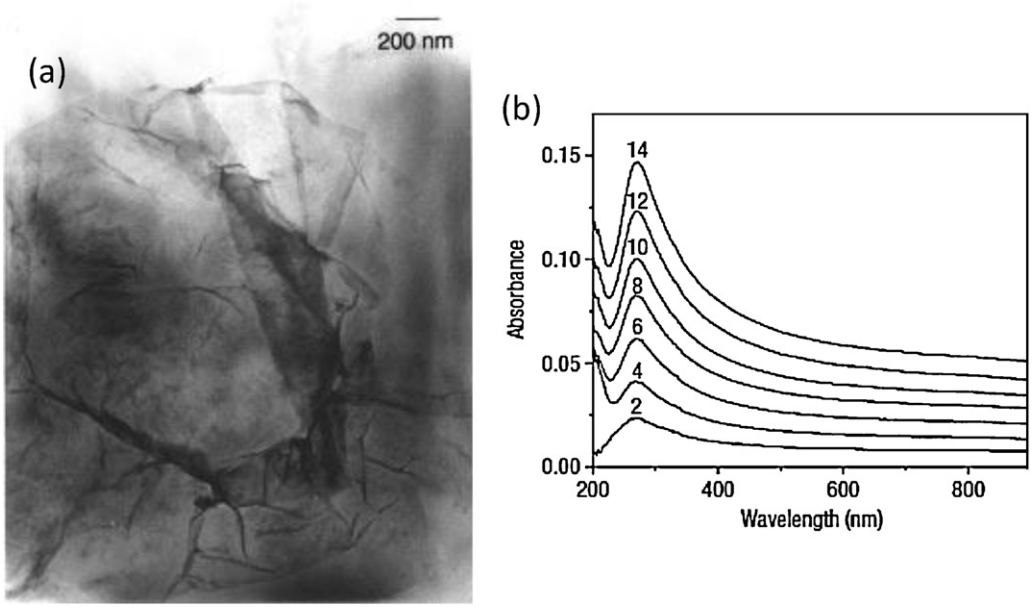

Figure 2 (a) Transmission electron micrograph of colloidal GO particles. Reprinted from Ref. [30] with permission by American Chemical Society. (b) UV—vis spectra of polycation/rGO films prepared by a LBL electrostatic self-assembly technique. The absorbance increases linearly with an increase in the number of assembly cycles (denoted above each curve), indicative of the successful assembly of rGO sheets on the substrate. Reprinted from Ref. [9] with permission by Nature Publishing Group.

acrylate)) (PDMAEA) and PAA modified rGO [36]. The $\pi-\pi$ stacking interaction between pyrene and rGO basal plane is the underlying mechanism for successful functionalization. The simple concept of LBL assembly also allows the incorporation of charged block copolymer into rGO multilayers [37].

Applications of SPG multilayers

Transparent conducting films (TCFs)

The highly aromatic 2D graphene with its exceptionally low intrinsic electrical resistivity is a potential candidate as a novel transparent electrode material if stacked thin enough (monolayer of graphene absorb ca. 2.3% of white light [38]). For graphene based TCFs, there is a trade-off between the transmittance (Tr) and sheet resistance (R_s), which are important parameters for practical applications of TCFs in displays, solar cells, etc. [39]. Increasing the thickness of graphene film will reduce Tr and R_s simultaneously. SPG with less ordered structures may not be the ideal candidate for TCFs, however, the combination of SPG with conducting polymers [40] or CNTs [41,42] and effective post treatment [13] have been shown effective in the increase of conductivity.

The earlier studies mainly focused on how to improve the conductance of the SPG multilayers. Kotov et al. accomplished the reduction of GO in thin film to improve the conductivity [11]. The reduction of GO in the $(PDDA/GO)_{10}$ film was achieved either chemically or electrochemically and the electrochemical reduction of GO film was found to be an irreversible process. The lateral resistance of $(PDDA/GO)_{10}$ film (measured between two 3 mm wide gold stripes evaporated on a glass slide at a separation of 2 mm) is 32 MΩ. After reduction by hydrogen, this value dropped to 12 kΩ, which corresponds to a change in volume conductivity from $1.2 \times 10^4\ \Omega^{-1}\ m^{-1}$ to $3.1 \times 10^7\ \Omega^{-1}\ m^{-1}$. Szabo et al. further reported that post heat treatment at 400 °C in air could improve the 3D ordering of adjacent rGO layers and in turn decrease the resistivity of the film [43]. The modification of GO with cetyltrimethyl ammonium bromide (CTAB) allows its assembly with negative charged polymers, such as PAA [44] and poly(styrenesulfonate) (PSS) [45]. The conductivity of PAA/CTAB-GO multilayer was found to be 60 S cm^{-1} compared with that of 200 S cm^{-1} in PSS/rGO multilayers. The authors observed that the conductivity of these multilayers is related to the number of the bilayers. Recently, the same group used spin-assisted LBL assembly to prepare (PSS/CTAB-rGO/sodium dodecyl sulfate (SDS)-rGO) multilayered film. They found that high rotation speed coupled with small sized rGO nanosheets could produce thin films with low percolation threshold and high conductivity (80—110 S cm^{-1}) [46]. Improvement in the conductivity of multilayered film formed by stacking of GO with exfoliated layered double hydroxide (LDH) nanosheets was also observed after the reduction of GO into rGO [47].

Recently, Lee et al. demonstrated the application of SPG thin film assembled with oppositely charged rGO as a transparent, conducting electrode for an organic light emitting diode, however, the performance was found to be inferior to ITO [48]. R_s of 2.5 kΩ/sq is obtained at Tr of 75%. It is worthy pointing out that an annealing process at 1000 °C in H_2 atmosphere is necessary to decrease R_s to a level enough for the conducting electrode. Park et al. reported R_s of 1.4 kΩ/sq with Tr of 80% after thermal treatment under argon atmosphere of rGO multilayers [49]. The thermal treatment was found to be crucial for the decrease of R_s due to the removal of functional groups. Similarly, the post annealing process also improved the conductivity of PAH-rGO/PSS-rGO

multilayers [50]. After the film was annealed at 250 °C under nitrogen atmosphere for 2 h, it exhibited a conductivity of 0.2 S cm^{-1} and R_s of 30 kΩ/sq. The integration of multi-walled nanotubes (MWNTs) with rGO nanosheets was also possible by using positively charged MWNTs and negatively charged rGO nanosheets [51]. The structure is characterized by the network of conductive MWNTs bridging the rGO nanosheets. The hybrid multilayer exhibited R_s of 8 kΩ/sq with a Tr of 81% after the thermal treatment.

It is necessary to point out that the above examples from LBL assembled SPG films all fell well short of ITO [52] unlike those for carbon nanotubes [53,54]. There may be two reasons for the poor performance: (1) the presence of inter-flake tunneling barriers, (2) the presence of large amounts of functional groups in SPG that are hard to be removed completely by existing reduction methods. We could get some clues from the results reported from CVD grown graphene [55—57]. Quasi-continuous graphene with highly ordered structure could dramatically decrease the quantity of tunneling barriers between flakes. A polymer-assisted transfer process for graphene grown by CVD method resulted in R_s of 54 Ω/sq and Tr of 85% with the $AuCl_3$ doping [56]. A further improvement was achieved in the roll-to-roll production of graphene films. TCFs with R_s of 30 Ω and Tr of 90% were obtained by the transfer of graphene film on copper foil to a polymer substrate and nitric acid doping [57]. Comparison with other solution-based method shows that the TCF performance of LBL assembled SPG is in most cases on par with that of films made by vacuum assisted flocculation (VAF) [41,58—62], dip-coating [16] and LB assembly [15], with typical R_s in the order of several kΩ (Table 1). The current spin-coating technique gives better results with the smallest R_s of 80 Ω [40], however, it is hard to attribute this to the technique itself, because the composition of the film and the post treatment between different methods are usually not comparable. We note that the involvement of insulating compositions as partners of SPG during LBL assembly should be avoided if possible for better TCF performance and the chemical modifications of SPG should be kept to a minimum.

Field effect transistors (FETs)

The high carrier mobility in graphene sheets makes them attractive material for FETs [28]. However, the solution-based technique unavoidably introduces impurities, defects, and dopants, which greatly diminish FET performance. Also, the limitation of the uniformity of SPG along with the difficulty in bridging source and drain terminals by large area single layer SPG principally lowers the overall mobility in SPG multilayer based FETs due to scattering at the junctions of overlapping nanosheets. Thanks to the exclusion of sheet junction effects, the carrier mobility of FETs based on single layer of SPG is generally superior to multilayers [63].

In order to open the band-gap of semi-metal graphene for a practical on/off ratio, one can produce narrow ribbons (the decrease of carrier mobility is anticipated [64]). Zhu et al. fabricated LBL assembled thin film from chemically modified graphene nanoribbons (GNRs) [65]. GNRs were prepared by using the CNT unzipping technique where MWNTs were treated with potassium permanganate in acid and were subsequently functionalized based on diazonium chemistry. The functionalized charged GNRs allowed the fabrication of thin film FET under ambient conditions. Unlike many ambipolar graphene [28] or rGO [58] FETs, the GNRs thin film FET showed only p-type behavior, suggesting the effect of functional groups on the GNRs thin film was p-doping. The possibility of generating band gaps through quantum confinement is ruled out because the GNRs used in this work have large widths of over 100 nm. The hole mobilities (μ_h) of 0.1—0.5 cm^2/(V s) were obtained and the on/off ratio was very low compared to FET transistors based on single nanoribbon [64].

Table 1 Comparison of TCF performance.

Method	Source	R_s	Tr (550 nm)	Post treatment	Ref.
LBL assembly	rGO/MCNTs	8 kΩ	81%	1000 °C, H_2	[51]
LBL assembly	rGO	2.5 kΩ	75%	1000 °C, H_2	[48]
LBL assembly	rGO	1.4 kΩ	80%	300—900 °C, Ar	[49]
LBL transfer	CVD growth G	90 Ω	80%	Nitric acid doping	[55]
LBL transfer	CVD growth G	54 Ω	85%	$AuCl_3$ doping	[56]
LBL transfer	CVD growth G	30 Ω	90%	Nitric acid	[57]
Vacuum filtration	GO	100 kΩ	90%	Hydrazine reduction and 200 °C, N_2	[58]
Vacuum filtration	Liquid exfoliated *G*	3.5 kΩ	80%	Nitric acid	[59]
Vacuum filtration	rGO/(PEDOT:PSS)	2.3 kΩ	80%	$SOCl_2$	[60]
Vacuum filtration	rGO	2.2 kΩ	80%	$HAuCl_4$	[61]
Vacuum filtration	rGO	2 kΩ	80%	1100 °C, Ar	[62]
Vacuum filtration	Liquid exfoliated *G*/CNTs	100 Ω	80%	Nitric acid	[41]
Spin-coating	rGO/CNTs	240 Ω	86%	$SOCl_2$	[42]
Spin-coating	GO	100 Ω	80%	1100 °C, vacuum	[13]
Spin-coating	rGO/(PEDOT:PSS)	80 Ω	80%	150 °C, air	[40]
Dip-coating	rGO	11.3 kΩ	87%	200 °C, Ar	[16]
LB	Liquid exfoliated *G*	8 kΩ	83%[a]	350 °C, air	[15]

[a] Defined as transmittance at a wavelength of 1000 nm.

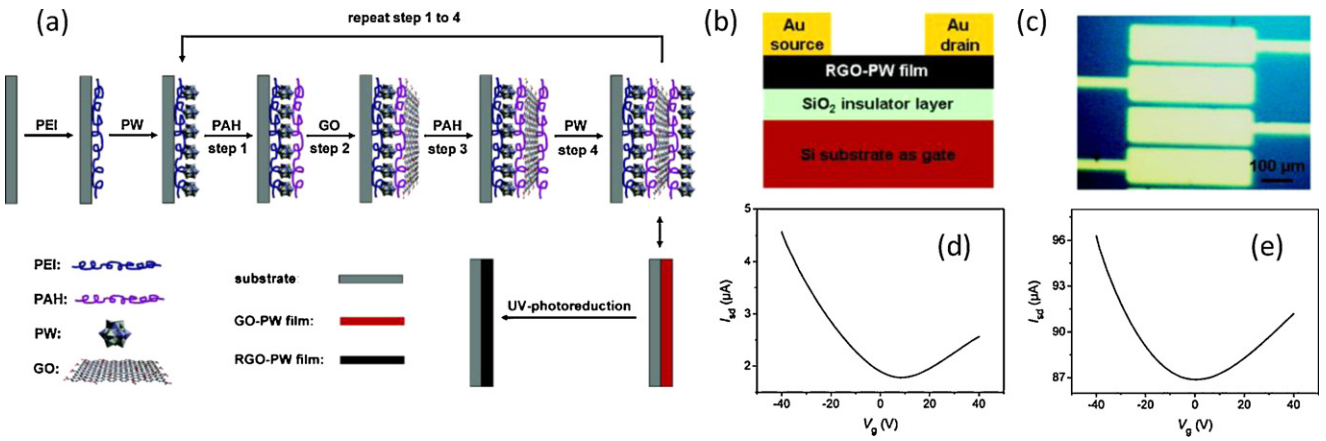

Figure 3 (a) Schematic illustration of the fabrication procedure of rGO-PW multilayer films, which involves the LBL assembly of GO nanosheets and PW clusters using cationic polyelectrolytes polyethylenimine (PEI) and PAH as electrostatic linkers, and a subsequent in situ photoreduction to convert GO to rGO. (b) rGO-PW film-based FET devices (cross section). (c) Optical microscope image of the actual device (top view). The blue part is the surface of the rGO-PW films. The Au electrodes appear bright. (d) and (e) I_{sd}—V_g curves of the FET devices fabricated on a (PAH/GO/PAH/PW)1 film (d) and a (PAH/GO/PAH/PW)6 film (e). Both samples were prepared on PEI/PW precursor film-modified silicon substrates with 300 nm thermal oxide and underwent 6 h of UV photoreduction. V_{sd} = 10 V.
Reprinted from Ref. [66] with permission by American Chemical Society.

Recently, Li et al. fabricated multilayers of GO nanosheets and $H_3PW_{12}O_{40}$ (PW) clusters with PAH as a linker, a subsequent in situ photoreduction procedure then converted GO to rGO due to the photocatalytic activity of PW [66] (Fig. 3a). Thin film FETs based on these multilayered films showed typical ambipolar characteristics and good transport properties for both electrons and holes (Fig. 3b—e). Hole and electron mobility values of $\mu_h = 0.03$ and $\mu_e = 0.01\ cm^2/(V\,s)$ for $(PAH/GO/PAH/PW)_1$ film, and $\mu_h = 0.15$ and $\mu_e = 0.06\ cm^2/(V\,s)$ for $(PAH/GO/PAH/PW)_6$ film were obtained. The on/off ratio of $(PAH/GO/PAH/PW)_1$ film device was ~2.0, and that of $(PAH/GO/PAH/PW)_6$ film device was ~1.1. Although these results indicate that the performance of FET can be easily tailored by controlling the number of layers in LBL assembly, the reported mobilities from solution-based methods [58,64,67—73] including LBL assembly [65,66] (usually with a back-gate of Si/SiO_2) are orders of magnitude smaller than mechanically exfoliated [28,74,75], CVD [4,76,77] and epitaxial grown [5,78] graphene transistors. A possible way to improve the transport properties of SPG is ionic screening, which could improve the carrier mobilities by up to $5000\ cm^2/(V\,s)$ [79].

Lithium ion batteries (LIBs)

Most of the research efforts for the application of SPG in LIBs aim at improving the performance of anode materials via the replacement of commercial graphite, which has a limited theoretical specific capacity of 372 mA h/g (C_6Li) [80]. Graphene is suggested to have twice as many low energy lithium sites as graphite due to the host of Li ions in both sides (C_3Li) [81]. This capacity could be further boosted by the suggested covalent Li_2 sites (C_2Li) [82] and the low energy edge sites ($C_{1.5}Li$) [83]. Elaborating on this reasoning, the presence of a great number of defects (vacancies, topological defects and impurities besides edge defects) in SPG introduced by the oxidation—reduction process [84—89] or doping [90—93] can serve as additional sites for lithiation, further improving the capacity to surpass the theoretical limit.

Typically, the fabrication of SPG based anode starts from the preparation of GO, which can be modified before or after separation from the solution [84—93]. The reported reversible specific capacity of SPG based anode has approached 1300 mA h g^{-1} in the initial 25 cycles under a low current rate (typically less than 100 mA/g) [85]. The fact that the low energy sites have to be fully reached by Li ions to realize the theoretical capacity makes it necessary to keep as many few-layer SPG as possible in the anode and to provide a controlled arrangement of SPG layers with a suitable interlayer spacing for double-layer Li ion. To this end, LBL assembly can be very effective. This advantage was realized by Cassagneau et al. who reported the construction of a high reversible specific capacity (1232 mA h g^{-1}), rechargeable lithium-ion battery based on a self-assembled polyethylene oxide (PEO), PDDA, and GO nanosheet [94] (Fig. 4). A lithium wire as counter electrode and $LiASF_6$ electrolytes in methyl formate/ethylene carbonate were used for the evaluation of cell performance. Concomitant with lithium-ion insertion, GO was found to be reduced to rGO. The use of PEO is critical according to the authors to facilitate the transport of Li ions to GO. The reported value of capacity ($C_{1.8}Li$) could be further improved if high temperature treatment is applied to reduce GO, thereby improving the conductivity. Nevertheless, the high capacity of this LBL assembled composite ranks at the top of the SPG based anode (300—1300 mA h g^{-1}) [84—93].

SPG has also been widely utilized in combination with other materials having large theoretical specific capacity as a conductive supporting material to withstand the large volume change of metal or metal oxides during charge—discharge process [95—103]. The intimate contact between SPG and other active materials is a prerequisite

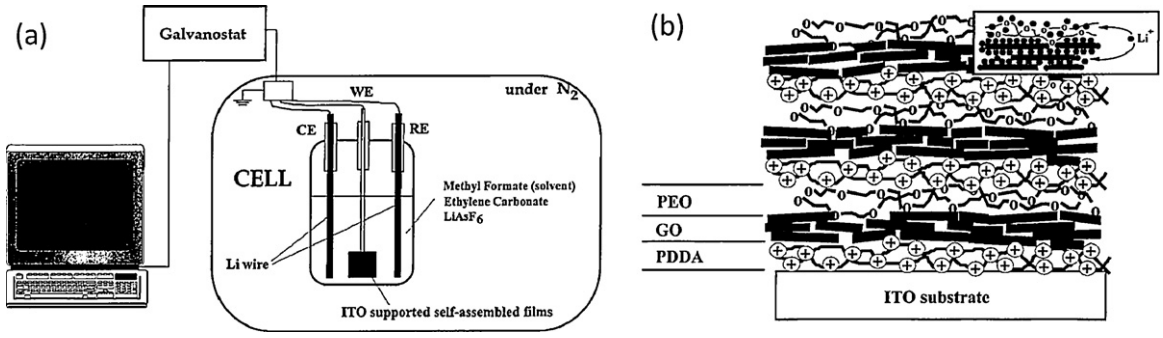

Figure 4 (a) Schematic of the self-assembled rechargeable LIB used for the electrical measurements. (b) Schematic of a self-assembled S-(PDDA/GO/PEO)$_3$ film. The box illustrates the intercalation of lithium ions into the GO and PEO layers (i.e. charging and concomitant reduction of GO to *G*).
Reprinted from Ref. [94] with permission by Wiley—VCH.

for superior synergetic results based on either simple mixing [100,103] or post assembly methods [95—99,101,102]. A LBL filtration method was reported for the preparation of rGO/MnO_2 nanotube composites [104]. However, the results are not optimized due to the lack of intrinsic interactions between different components and therefore there is still room for traditional LBL assembly to further the performance of SPG supported LIBs anode. It is worth mentioning that other than specific capacity, rate capability and cycling performance are also important factors in the evaluation of LIBs. A comprehensive analysis is needed before a suitable processing method is selected.

Supercapacitors

In contrast to LIBs in which energy storage is realized in the form of chemical reactions in the bulk electrode, significant accumulation of electrical energy can also be achieved at the electrode/electrolyte interface. This concept is the foundation of supercapacitors including electrical double layer capacitors (EDLCs) (non-Faradic) and pseudocapacitors (Faradic). Materials with large specific surface area (SSA) are widely used in supercapacitors including activated carbon, carbon aerogels and CNTs [105,106], nanostructured metal oxides [107] and conducting polymers [108]. Specific energy of the supercapacitors can reach 5—10 Wh/kg, which is approaching that of LIBs, i.e. 120—170 Wh/kg, while keeping excellent powder density (10—100 kW/kg). Given that graphene has a SSA as high as 2630 m^2/g, which is even higher than the SSA of CNTs 1600 m^2/g, the studies of graphene as supercapacitor electrodes are extensive [109]. Notably the conductivity of the electrode is an essential parameter for supercapacitors and SPG values lag significantly behind those for CNTs and theoretical values for graphene.

The specific capacity of EDLCs with SPG as the main active electrode material (SPG only or with other carbon materials) is in the range of 120—320 F/g. For SPG only electrodes, hydrogel from hydrothermal treatment (220 F/g) [110], thin film from vacuum assisted flocculation (VAF) (135, 187 F/g) [111,112] or dip-coating (211 F/g) [113], blend with typical binders (polytetrafluoroethylene, acetylene or carbon black) (135, 205 F/g) [114,115] were reported. A higher value of 247 F/g was achieved in LBL assembled polyethylenimine (PEI)/rGO film with an in-plane configuration to boost the ion absorption on edges and facilitate ion transport [116] (Fig. 5a and b). The interlayer distance was found to be 0.5 nm in multilayers of rGO, which is large enough to accommodate the counter-ions in polyvinyl alcohol (PVA)/H_3PO_4 gels. The combination of SPG, for example, with carbon spheres [117] or CNTs [17,118] showed promising results with high specific capacity of 318 F/g at a low current rate of 0.1 A/g from rGO/CNT hybrid hydrogel [118]. Although LBL assembly was believed to prevent the restacking of SPG more efficiently than solution blending [17,117,118], a study on self-assembled PEI-rGO/CNT film showed only a specific capacity of 120 F/g at 1 V/s [119]. The presence of insulating polymer in the film may be responsible for the relatively low capacity in contrast to the high value reported by Yoo et al. [116], where PEIs were removed before chemical reduction of GO.

The integration of SPG with metal oxide nanoparticles and conducting polymers could show a positive synergetic effect, considering the effective interface between active nanomaterials and SPG for charge transport is built up. Here the role of SPG in pseudocapacitors is similar to its role in LIBs. Hybrid structures of SPG with Fe_3O_4 [120], MnO_2 [121], $Ni(OH)_2$ [122], RuO_2 [123], etc. have been prepared by growing metal oxide nanostructures on SPG. Supercapacitors based on LBL assembled architectures of PSS-rGO/MnO_2 nanosheets (with PDDA as a linker) showed a specific capacitance of 263 F g^{-1} for the ITO/(PDDA/PSS-rGO/PDDA/MnO_2)$_{10}$ multilayers at a discharge current density of 0.283 A g^{-1} [124], on par with that from the seeded growth method [121] and superior to simple mixing [125]. Conducting polymers like polyaniline [126] and polypyrrole [127] can be combined with SPG by in situ polymerization in the presence of SPG. Alternatively, a LBL dip-coating method was used to prepare polypyrrole nanowires/SPG multilayered structures by transferring self-assembled film on the air/liquid interface [128]. The specific capacitance was found to be only 165 F g^{-1} which is at the lower end of reported polypyrrole/SPG based supercapacitors [127,129].

A comparison could be made between hybrid Co-Al-LDH/GO structures made by co-precipitation [130] and LBL assembly [131]. An improved specific capacity of 880 F/g

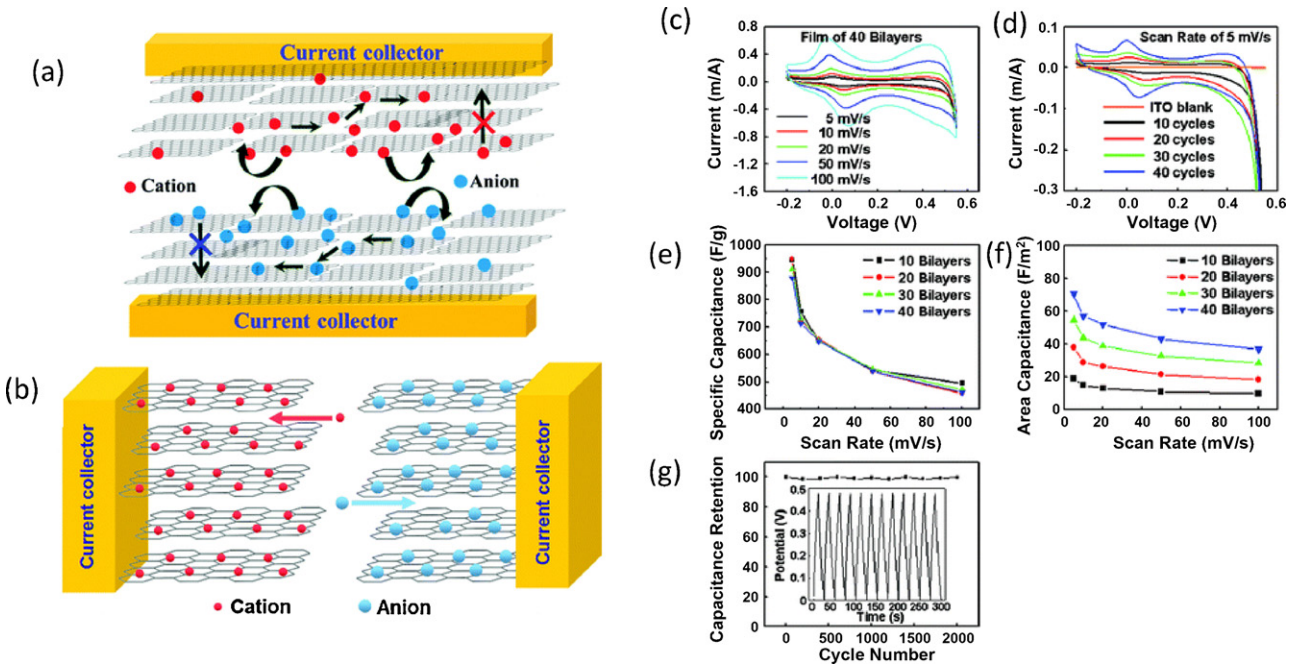

Figure 5 (a) Schematic depiction of the stacked geometry used for the fabrication of supercapacitor devices. Graphitic carbon-based materials are randomly oriented with respect to the current collectors in such a stacked geometry. In the case of the stacked (conventional) geometry the electrochemical surface area is incompletely utilized, because some of the regions are inaccessible to the electrolyte ions. (b) Schematic depiction of the operating principle in case of the in-plane supercapacitor device utilized for the performance evaluation of graphene as electrodes. The new architecture presents the added benefit of increased ability of the electrolyte to percolate into the layers of graphene to allow for full utilization of the electrochemical surface area. Reprinted from Ref. [116] with permission by American Chemical Society. (c) Cyclic voltammograms of a 40-bilayer film of Co—Al LDH/GO at various scan rates. (d) Cyclic voltammograms of bare ITO and four Co—Al LDH/GO films with 10, 20, 30, and 40 bilayers at a scan rate of 5 mV/s. (e) Specific capacitance and (f) area capacitance of the four films at various scan rates. (g) Galvanostatic charge and discharge curves and specific capacitance vs. cycle number at a current density of 20 A/g for the 40-bilayer Co—Al LDH/GO film. Reprinted from Ref. [131] with permission by American Chemical Society.

was obtained by LBL assembly (Fig. 5c—g) compared with 778 F/g by co-precipitation at 5 mV/s, which is a result of more ordered assembling of GO and Co-Al-LDH for efficient charge transport. It is not surprising to see the benefit of LBL assembly in the preparation of electrode for supercapacitors, as the consideration here is basically the same as in LIBs. For example, LBL assembled materials can minimize the restacking of SPG and engineer the inter-plate pore size for the accessibility of electrolyte. However, the careful selection of polymers and engineering of interfacial interactions must be considered, otherwise, the effect can be negative [128,132].

Solar cells

The extensive study of graphene-based transparent conductors promotes their applications as window electrodes in organic solar cells [133—137] and dye-sensitized solar cells (DSSCs) [138]. One of the benefits here is the wide absorption spectral range of graphene and SPG, which could potentially improve the power conversion efficiency (PCE). Also, the work function of graphene (4.5 eV) [139] can be varied by changing surface states [140,141] or number of layers [142] toward efficient carrier injection. The performance of graphene and SPG based TCFs in solar cells is usually behind that of canonical ITO [133—138], calling for the solution to higher conductivity, transparency, smoothness, and also better compatibility with active layers.

Other than transparent conductors, SPGs can also be used as active materials in DSSCs. When used as photocathode, the unique functionalities and high surface area of SPG could allow the replacement of precious Pt photocathode in DSSCs, forming transparent Pt-free cathodes [143]. Gong et al. showed that it is possible to use LBL thin film modified transparent electrode to reduce the Pt amount in counter electrode in DSSCs and keep comparable photovoltaic performance compared to sputtered Pt electrodes [144]. Multilayered structures of $(PDDA/rGO/PDDA/H_2PtCl_6)_n$ built on conductive fluorine doped tin oxide (FTO) glass were further sintered to generate rGO/Pt thin film. The comparative studies revealed that the rGO layers inserted between the FTO and Pt layer played a significant role in achieving good solar cell performance at a low cost of Pt. The PCE was reported to be around 6%, which is typical for DSSCs with a SPG photocathode (mainly fall within the range of 4—7%) [143,145—147]. SPGs can also be active electron acceptors in DSSCs, with PCE improvement from 30 to 60% [148—150], comparing with bare TiO_2 photoanodes. The electron-accepting ability further makes SPG a potential replacement of the commonly used [6,6]-phenyl C61-butyric acid methyl ester (PCBM) in bulk heterojunction

(BHJ) organic solar cells [151,152]. Interestingly, SPG was suggested to be an alternative hole transport layer in organic solar cells, thanks to its unique electronic structures [153,154].

The advantage of multilayered structure in solar cells was demonstrated by Guo et al. in quantum dot solar cells (QDSCs) using CdS/rGO thin film [155] (Fig. 6a and b). PCE can be improved from 5% for $(CdS/rGO)_2$ to 16% for $(CdS/rGO)_8$. Further increase of the number of bilayers will decrease PCE, which can be due to the combination effect of light absorption and charge transport. The reported PCE of 16% was far superior to other carbon material based QDSCs with PCE typically less than 5% [156—159] and also better than the performance of single-walled nanotube (SWNT) based multilayers (Fig. 6c and d). The large enhancement of PCE indicates that LBL assembled structures ensure a good distribution of CdS NPs and good contact with rGO, which results in an effective charge separation together with the favorable work function and high electron mobility of rGO. The ability to independently tune the property of each constituent layers renders a controllable way to improve the solar absorption and reduce the carrier recombination, both of which are important for higher PCE. The study on the electron transfer process in $Ti_{0.91}O_2$/rGO multistacked assemblies also indicated the high separation efficiency of photo-induced electrons and holes, which is manifested by the enhancement of the photocurrent [160].

Sensors

Graphene and SPG have attracted a lot of attention for sensing applications, mainly electrochemical, electronic, and optical sensors [161]. The high electron transfer rate, high carrier mobility, and fluorescence quenching ability along with the high surface area and outstanding mechanical properties make graphene and SPG strong competitors with CNTs [162]. SPG with modifiable and abundant functional groups, and edging reactive sites can be a more attractive candidate to concentrate analytes.

The detection of gases is usually based on the changes of conductance (chemiresistors) [163—165] or local carrier concentration (FETs) [166,167] induced by charge transfer between adsorbates and graphene or SPG. Single molecule level detection can be achieved based on mechanically exfoliated graphene for NO_2 [166]. Other aggressive gases including HCN (detection limit 70 ppb) [165] and DNT (detection limit 0.1 ppb [165] and 28 ppb [168]) can also be detected. Most of the graphene sensors can respond to vapor pressures well below that at room temperature. Besides

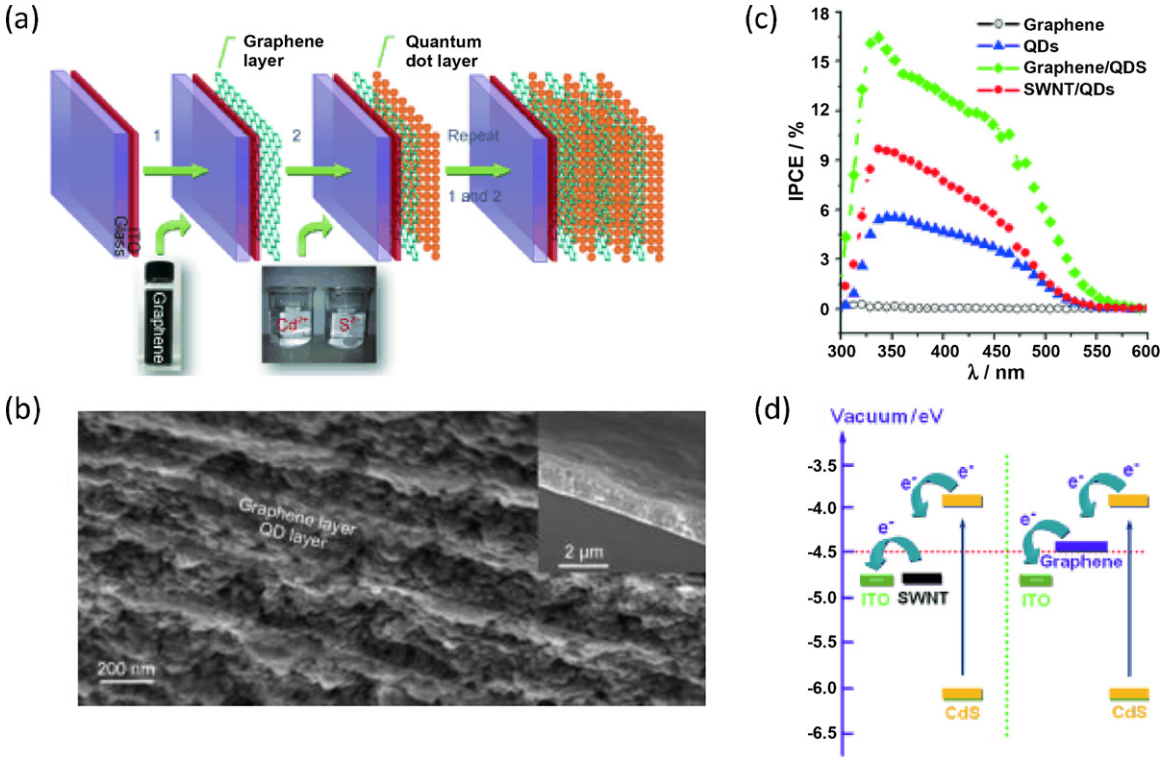

Figure 6 (a) Fabrication of the layered graphene/QDs on ITO glass. (1) Precleaned ITO glass was coated with a thin layer of graphene by electrophoretic deposition from aqueous solution of chemically reduced graphene. (2) Subsequently, a layer of CdS QDs was directly synthesized on predeposited graphene layer by sequential chemical bath deposition from their salt aqueous solutions. The layered graphene/QDs device was fabricated by repeating steps 1 and 2. (b) Cross-sectional SEM image of a $\{graphene/QDs\}_{10}$ sample. The inset shows its thickness. (c) Dependence of the incident photon conversion efficiency (IPCE, external quantum yield) on the incident wavelength of different photoelectrodes. (d) Energy-level diagram of the bilayer system.
Reprinted from Ref. [155] with permission by Wiley—VCH.

the sensing mechanism above, LBL assembly of SPG could readily provide 2D cavities that are ideal for molecular discrimination. For example, Ji et al. demonstrated selective gas sensing based on multilayered ionic liquid functionalized rGO/PSS film assisted by quartz crystal microbalances (QCM) [169]. A higher affinity for toxic aromatic hydrocarbons than for their aliphatic analogs was observed and the amount of adsorbed benzene depended significantly on the type of ionic liquid. Interestingly, rGO prepared without an ionic liquid component showed almost no adsorption capability. The authors suggested that the high affinity between rGO and certain kinds of ionic liquids is the key to achieve the nanospace formed between sp^2-hybridized carbon nanosheets with high selectivity of gases with different properties. However, the sensing test in this work that used saturated analyte vapors at room temperature could not give more information about the detection limit and sensitivity. The combination of SPG with active catalysts further extends the sensing target of gases. Zhu et al. reported the electrocatalytic activity toward oxygen based on rGO/Pt multilayer modified electrode [170].

LBL assembled SPG multilayers are also used in the detection of H_2O_2 (an enzymatic product of many biological processes) based on the electrochemical method. Mao et al. used functionalized, ionic liquid modified, rGO nanosheets and Prussian blue (PB) nanoparticles to fabricate multilayered film with a detection limit of up to 1 μM [171]. Further improvement is possible by using thionine-functionalized rGO nanosheets in gold nanoparticles/horseradish peroxidase (HRP) multilayer [172]. The as-prepared multilayered biosensor exhibited high sensitivity, good reproducibility and selectivity. Linear response was obtained for the range from 0.5 μM to 1.8 mM of H_2O_2, the detection limit is 10 nM, and 95% of the steady state current was reached within 2 s. The method was also demonstrated to be successfully applied to detect H_2O_2 in spiked sterilized milk. The impressively low detection limit (10 nM) surpasses many SPG based sensors, including 0.51 μM for rGO/chitosan with hemoglobin (Hb) [173], 0.1 μM for HRP/sodium dodecylbenzenesulfonate (SDBS)-rGO [174], 80 nM for Pt NPs/rGO [175], and 45 nM for rGO/PB [176]. Further sensing function for glucose was reported based on PEI/pyrene-grafted PAA modified rGO multilayers [177]. A glucose biosensor could be fabricated by depositing glucose oxidase/PEI multilayers on the top of rGO multilayers. The detection limit and sensitivity were determined to be 0.168 mM and 0.261 $\mu A\,mM^{-1}\,cm^{-2}$, respectively. The performance still needs to be optimized in order to compete with other SPG based glucose sensors with better detection limits (as low as 0.6 μM) [178]. Recently, Wang et al. fabricated multilayered nanostructures of rGO/methylene green (MG) and rGO/MWNTs onto glassy carbon (GC) electrodes by LBL assembly [179]. The modified electrodes showed good electrocatalytic activity toward the oxidation of nicotinamide adenine dinucleotide (NADH), comparable with MG/SWNTs modified electrodes [180].

In addition to the sensors mentioned above, SPG could function as biosensors for the detection of biomolecules including DNA and protein markers based on electronic [181—183], electrochemical [184—186], or optical procedures [187,188]. The specific recognition between biomolecules (antigen-antibody) is an important action mechanism. Recently, the flexible cancer sensor with ultrahigh sensitivity was demonstrated based on LBL assembled $(PDDA/PSS)_2(PDDA/graphene)_5$ multilayers [189] (Fig. 7a—d). Different working mechanisms are responsible for label-free and labeled graphene based biosensors: in label free state, the conductance of the biosensor modified with the prostate specific antigen (PSA) capture antibody shifts with the concentration change of PSA solutions; in the labeled state, the HRP conjugated with PSA antibody catalyzes a biochemical reaction by the mixture of ascorbic acid (AA) and H_2O_2, the resultant change of local pH induces the conductance variation of the biosensor. It is encouraging to see that the graphene based sensors in this work are generally better than CNT sensors under the same conditions with the capability to detecting very low concentrations of PSA down to 4 fg/ml (0.11 fM) (label-free) (Fig. 7e) and 0.4 pg/ml (11 fM) (labeled), respectively. The high quality of the graphene crystal lattice and 2D structures, which tend to screen charge fluctuations more than 1D system, is critical for the achievement of the very low detection limit which is three orders of magnitude lower than CNT sensors (Fig. 7f). The record detection limit outperforms other SPG based sensor [190] and sensing systems [191—194]. An interesting photoelectrochemical sensor was demonstrated by Zhang et al. for the detection of thrombin based on rGO/CdSe NPs multilayered film which was modified by DNA aptamer [195]. The sensing mechanism was based on the formation of aptamer-thrombin complex that could block the diffusion of the sacrificial electron donor (AA) to the surface of the electrode and lead to a decrease of photocurrent. The electron-accepting ability of rGO enhanced the electron transport and thus impeded the charge recombination of excited CdSe, resulting in the improved photo-responses. A detection limit of 4.5 pM was reported.

Polymer nanocomposites

The excellent mechanical properties of graphene make it an attractive reinforcing agent in polymer nanocomposites. The cost-effective mass production of SPG by solution method and their surface groups available for functional modifications give more credit to SPG when used as fillers, which could potentially replace CNTs [196] or form their hybrids [197]. The mechanical properties of polymer nanocomposites not only rely on the intrinsic properties of SPG [198,199], but also their dispersion degree in and interaction with polymer matrix. As the surface of SPG is more hydrophilic, the combination of SPG with for example, PVA [200], cellulose [201,202], chitosan [203] and waterborne polyurethane [204], could adopt solution blending method. In situ polymerization, which usually involves surface grafting, is more frequently used for hydrophobic polymers such as nylon [205], polyimide [206], and epoxy [207]. Melt mixing was also investigated [208], but the outcome was inferior to the solution compounding [209]. For more information about this subject, readers can refer to several recent reviews [210—212].

Here we will focus on the PVA/SPG system to compare the composite film prepared by LBL assembly and other methods. The existence of oxygen functional groups located on both edges and basal planes enables hydrogen bonding

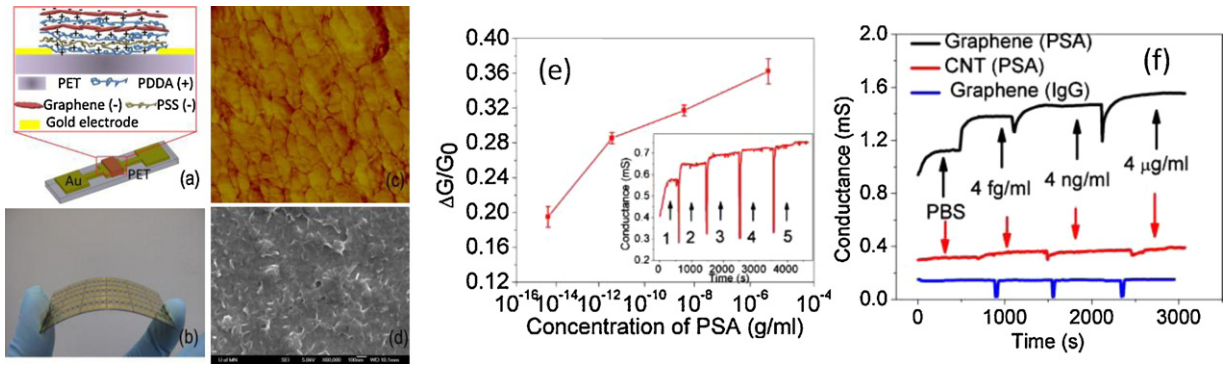

Figure 7 (a) Schematic illustration of LBL self-assembled *G* nanocomposite before immunization. (b) Optical image of LBL self-assembled *G* cancer sensor on a flexible PET substrate. (c) AFM image of LBL self-assembled (scanning area is 1 μm × 1 μm). (d) SEM image of LBL self-assembled *G* displaying its porous defoliation surface profile. The average *G* nanoplatelet is about 100 nm × 100 nm. (e) Shift in normalized conductance vs. PSA concentration for label-free *G* sensors. Inset: conductance vs. time data recorded after alternate delivery of the following concentrations of PSA: (1) PBS contains no PSA, (2) 4 fg/ml, (3) 4 pg/ml, (4) 4 ng/ml, and (5) 4 μg/ml. Initial conductance G_0 represents the *G* conductance in PBS solution, and other conductance tested under different PSA concentrations subtract G_0 to get ΔG. (f) Conductance vs. time testing for *G* and CNT biosensors with different PSA concentrations. The results demonstrate that the detection limit of *G* sensor is down to 4 fg/ml, compared with the CNT sensor with a detection limit of 4 ng/ml. In addition, various concentrations of normal rabbit IgG were delivered to the *G* sensor immunized with PSA capture antibodies, and the conductance of *G* sensor was kept constant.
Reprinted from Ref. [189] with permission by American Physical Society.

between SPG and PVA, which also makes LBL assembly of PVA and GO possible. A 98.7% improvement of Young's modulus (*E*) and a 240.4% increase of hardness (*H*) were reported in $(PVA/GO)_{300}$ thin film, with *E* at 17.64 GPa estimated by nanoindentation test [213] (Fig. 8a). Another nanoindentation study reported a maximum increase of 35 and 45% in the *E* and *H* of solution casted PVA/GO film, with *E* at 0.885 GPa [214]. The advantage of LBL assembly based on the comparison of these two studies is obvious and could be attributed to highly efficient load transfer. Other studies including solution casting [200,215—218] and vacuum assisted flocculation (VAF) [219] use tensile test to evaluate the mechanical properties, with the reported *E* in the range of 0.5—8 GPa. Although the reported *E* (17.64 GPa) in LBL assembled film is the highest value [213], the increase of *E* compared with pure polymer film has been reported

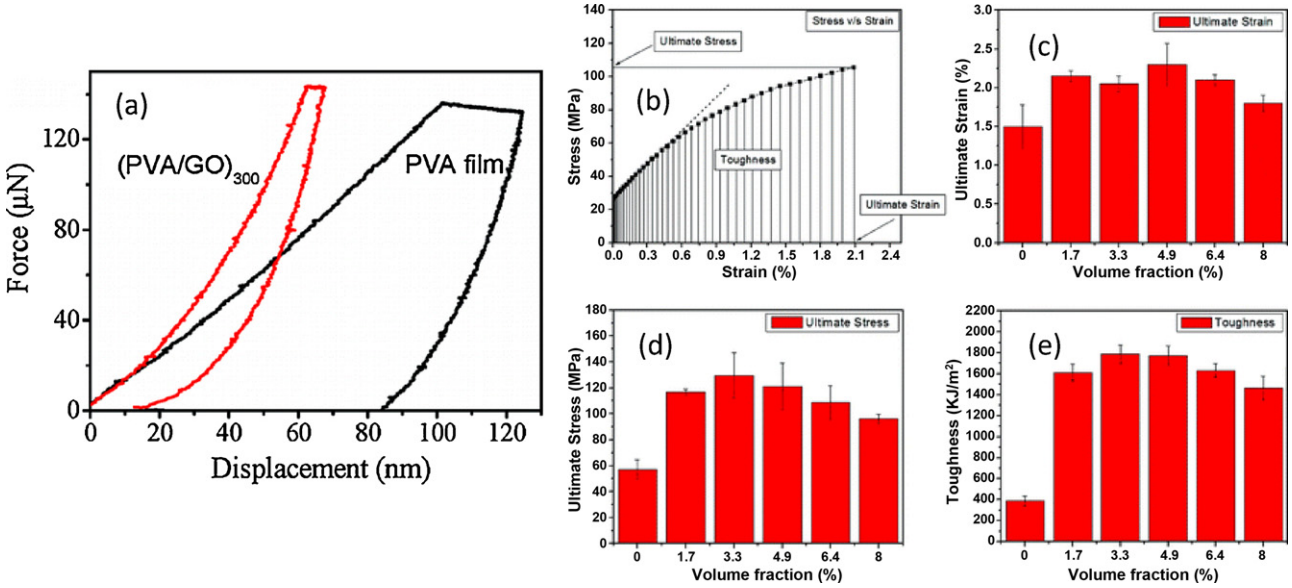

Figure 8 (a) Typical loading—hold—unloading curves of pure PVA film and LBL assembling $(PVA/GO)_{300}$ film. Reprinted from Ref. [213] with permission by American Chemical Society. (b) Representative stress vs. strain plot showing the ultimate strain, ultimate stress, and toughness values of GO involved PAH/PSS layered film. Variation of (c) ultimate strain, (d) ultimate stress, and (e) toughness with the volume fraction of GO component. Reprinted from Ref. [222] with permission by American Chemical Society.

to be 128—180% for other methods [217—219], and one paper reported as high as 10 folds improvement in a solution casting system [215], better than the improvement in LBL assembled film. This deviation implies the importance of other parameters such as polymer structure, water content [12,220,221] and surface chemistry of SPG in determining the mechanical properties of the composites. It is also possible to combine LBL assembly with LB method to fabricate free-standing, layered nanocomposites consisting of GO nanosheets sandwiched between PAH/PSS layered film [222]. The film was found to have excellent toughness and elastic modulus, reaching 1.9 MJ/m^3 and 20 GPa, respectively, for a low content of GO (about 8%), measured by buckling and bulging experiments (Fig. 8b—e). Considering the structural similarity between clay and SPG, and the success of using LBL assembly to prepare polymer/clay ultrastrong film [223], there should still be space to further improve the mechanical performance of LBL assembled SPG based polymer nanocomposites.

Comparative evaluation and prospects

The planar structure of SPG makes it ideal for assembly on substrates, during which energy minimization allows the nanosheets to self-organize parallel to each other in a way reminiscent in many biocomposites. Among other methods capable of producing such nanoscale morphology, LBL assembly is assumed to give more compact and ordered structures compared to other solution-based methods. This advantage comes from the rinsing steps and elimination of phase separation making possible optimization of interactions at the polymer—filler interface with better control over the forces than other techniques. In turn, this brings out the ability to carry out a function-dedicated nanoscale design of film structure down to the single-layer level. In some cases it is also significant that, compared to VAF, for instance, the requirement of being soluble in a common solvent is not relevant for LBL.

The comparison made in this review shows that the record properties come from LBL assembly, for example, in regards to the reversible specific capacity of LIBs, PCE in QDSCs and detection limit for PSA and *E* for PVA/SPG nanocomposites. However, in most cases, it is not certain that LBL assembled SPG multilayers would outperform materials made by other methods which appeared only recently given sufficient time spent on their optimization. As discussed, in TCF and FET, LBL assembled multilayers do not give record performance so far. Even for supercapacitors, the application which would be particularly good choice for LBL assembly due to high uniformity and interconnectivity of the charge-conducting components, the overall results are not competitive. Note, however, that new advantages of LBL can also be tapped in, which are not available in other techniques. For these kind of devices, stratification of the charge-conducting layers, by other words, the intrinsic gradient of, for instance conduction and valence band position in the films [224,225], can make substantial difference, which was demonstrated relatively recently [226,227].

Applications of SPG multilayers being discussed in literature are numerous (Fig. 9a). All of them need different designs of materials, which bears well with the materials engineering capabilities of LBL assembly that include an unprecedented variety of different components as constituents of the multilayers and its compatibility with the

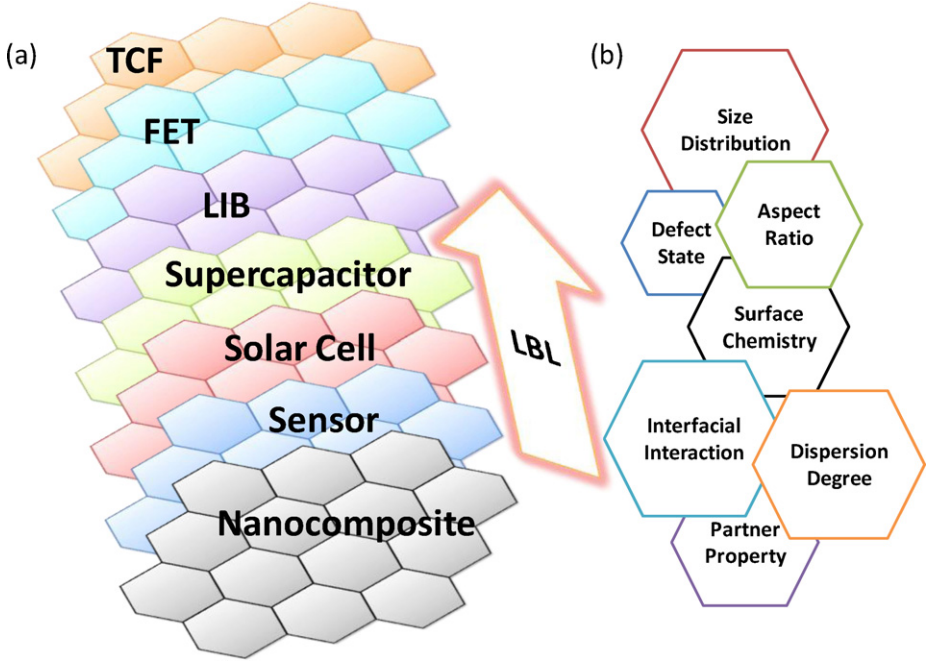

Figure 9 (a) Summary of the applications of LBL assembled SPG multilayers and (b) the key points toward better performance.

surfaces of any kind and any shape. Regardless of that, it is worth mentioning some common considerations which we believe are important for the achievement of properties for many of these applications (Fig. 9b) that can potentially push the envelope of corresponding technologies even further. (1) The source of SPG is a big concern. High quality SPG with a large aspect ratio, narrow size distribution and few-layer nature will be a benefit. Apparently, the high surface area of SPG originates from their thinness and large lateral dimension and the minimization of the defects when stacked upon each other due to the scattered spatial distribution and misalignment would need uniform sized SPG. Also, the defects of SPG need to be better understood and properly controlled under different circumstances. (2) The surface chemistry of SPG is another important factor. The versatile grafting chemistry allows desirable functional modification, however, the presence of these extraneous surface groups could interrupt the conjugation of the basal plane. There is a balance between the optimization of the interfacial interaction and the preservation of intrinsic properties of SPG. (3) Compared with other solution based method, the way of using a partner material in LBL assembly is unique. In principle, the selection of the partner for SPG aims at boosting the interfacial interactions, however, the incorporation of another part into SPG multilayers would possibly bring in unwanted materials for specific applications. For example, in electronic applications, a more conductive partner would be desirable, however, in nanocomposites, a stronger and tougher polymer might be needed. A good selection would be made based on the request. (4) The dispersion degree of SPG could be largely improved by LBL assembly, during which the interface engineering could be achieved. This advantage comes from the stepwise growth of the film, however, studies have shown that more than one layer thick growth of each SPG layer. Care should be taken to the concentration of SPG dispersion and dipping time.

The potential of all materials preparation techniques resulting in bimimetic assemblies of platelets could be further utilized in the exploration of novel applications for SPG multilayers. Diverse materials could be incorporated. The introduction of graphene quantum dots, novel metallic (such as gold and palladium NPs) and semiconductor nanostructures (such as CdTe and ZnO NPs), other 2D materials (such as BN and MoS_2 nanosheets) and unique polymer structures (such as cellulose and Kevlar nanofibers [228]) into the system of LBL assembled SPG multilayers will likely bring new opportunities for optical, electrical, sensing and mechanical applications. Other than that, the exploration of the thermal and barrier properties of current LBL assembled SPG multilayers may also be interesting topic.

Undoubtedly, there is still much space to fully take the advantage of nature-inspired materials assembly techniques for SPG multilayers. While the comparison of LBL assembly to other methods is important, we believe that the integration of different techniques will be the ultimate solution to practical and efficient device fabrication. We already see that LBL assembly has been blended with spin-coating, VAF, LB assembly, etc. The compatibility of materials assembly techniques with modern manufacturing processes such as micromanufacturing represented by traditional [229], maskless [230] and 3D lithography [231] is indispensible for the further development of these methods.

Acknowledgements

This material is based upon work largely supported by the Center for Solar and Thermal Energy Conversion, an Energy Frontier Research Center funded by the U.S. Department of Energy, Office of Science, Office of Basic Energy Sciences under Award Number #DE-SC0000957. This work was also supported in part by the Center for Photonic and Multiscale Nanomaterials (C-PHOM) funded by the National Science Foundation Materials Research Science and Engineering Center program DMR 1120923. We acknowledge as well the essential support from NSF under grant ECS-0601345; EFRI-BSBA 0938019; CBET 0933384; CBET 0932823; and CBET 1036672. The work is also partially supported by AFOSR MURI 444286-P061716, Army SBIR project A10-123, and NIH 1R21CA121841-01A2. The authors thank the University of Michigan's EMAL for its assistance with electron microscopy, and for the NSF grant #DMR-9871177 for funding for the JEOL 2010F analytical electron microscope used in this work. M.Y. thanks Rishi Goel for tidying up English writing.

References

[1] A.K. Geim, K.S. Novoselov, Nat. Mater. 6 (2007) 183—191.
[2] J.H. Chen, C. Jang, S.D. Xiao, M. Ishigami, M.S. Fuhrer, Nat. Nanotechnol. 3 (2008) 206—209.
[3] C. Lee, X.D. Wei, J.W. Kysar, J. Hone, Science 321 (2008) 385—388.
[4] X.S. Li, W.W. Cai, J.H. An, S. Kim, J. Nah, D.X. Yang, R. Piner, A. Velamakanni, I. Jung, E. Tutuc, S.K. Banerjee, L. Colombo, R.S. Ruoff, Science 324 (2009) 1312—1314.
[5] Y.M. Lin, C. Dimitrakopoulos, K.A. Jenkins, D.B. Farmer, H.Y. Chiu, A. Grill, P. Avouris, Science 327 (2010) 662.
[6] Y. Hernandez, V. Nicolosi, M. Lotya, F.M. Blighe, Z. Sun, S. De, I.T. McGovern, B. Holland, M. Byrne, Y.K. Gun'ko, J.J. Boland, P. Niraj, G. Duesberg, S. Krishnamurthy, R. Goodhue, J. Hutchison, V. Scardaci, A.C. Ferrari, J.N. Coleman, Nat. Nanotechnol. 3 (2008) 563—568.
[7] W.S. Hummers, R.E. Offeman, J. Am. Chem. Soc. 80 (1958) 1339.
[8] S. Stankovich, R.D. Piner, X.Q. Chen, N.Q. Wu, S.T. Nguyen, R.S. Ruoff, J. Mater. Chem. 16 (2006) 155—158.
[9] D. Li, M.B. Mueller, S. Gilje, R.B. Kaner, G.G. Wallace, Nat. Nanotechnol. 3 (2008) 101—105.
[10] C. Gomez-Navarro, R.T. Weitz, A.M. Bittner, M. Scolari, A. Mews, M. Burghard, K. Kern, Nano Lett. 7 (2007) 3499—3503.
[11] N.A. Kotov, I. Dekany, J.H. Fendler, Adv. Mater. 8 (1996) 637—641.
[12] D.A. Dikin, S. Stankovich, E.J. Zimney, R.D. Piner, G.H.B. Dommett, G. Evmenenko, S.T. Nguyen, R.S. Ruoff, Nature 448 (2007) 457—460.
[13] H.A. Becerril, J. Mao, Z. Liu, R.M. Stoltenberg, Z. Bao, Y. Chen, ACS Nano 2 (2008) 463—470.
[14] S. Gilje, S. Han, M. Wang, K.L. Wang, R.B. Kaner, Nano Lett. 7 (2007) 3394—3398.
[15] X.L. Li, G.Y. Zhang, X.D. Bai, X.M. Sun, X.R. Wang, E. Wang, H.J. Dai, Nat. Nanotechnol. 3 (2008) 538—542.
[16] Y.W. Zhu, W.W. Cai, R.D. Piner, A. Velamakanni, R.S. Ruoff, Appl. Phys. Lett. 95 (2009) 103104.
[17] S.H. Aboutalebi, A.T. Chidembo, M. Salari, K. Konstantinov, D. Wexler, H.K. Liu, S.X. Dou, Energy Environ. Sci. 4 (2011) 1855—1865.
[18] P. Podsiadlo, B.S. Shim, N.A. Kotov, Coord. Chem. Rev. 253 (2009) 2835—2851.

[19] S. Srivastava, N.A. Kotov, Acc. Chem. Res. 41 (2008) 1831—1841.
[20] G. Decher, Multilayer Thin Films, Wiley—VCH Verlag GmbH & Co. KGaA, 2012, pp. 1—21.
[21] A. Lerf, H.Y. He, M. Forster, J. Klinowski, J. Phys. Chem. B 102 (1998) 4477—4482.
[22] T. Cassagneau, F. Guerin, J.H. Fendler, Langmuir 16 (2000) 7318—7324.
[23] W. Gao, L.B. Alemany, L.J. Ci, P.M. Ajayan, Nat. Chem. 1 (2009) 403—408.
[24] S. Park, R.S. Ruoff, Nat. Nanotechnol. 4 (2009) 217—224.
[25] S. Stankovich, D.A. Dikin, R.D. Piner, K.A. Kohlhaas, A. Kleinhammes, Y. Jia, Y. Wu, S.T. Nguyen, R.S. Ruoff, Carbon 45 (2007) 1558—1565.
[26] X.M. Sun, Z. Liu, K. Welsher, J.T. Robinson, A. Goodwin, S. Zaric, H.J. Dai, Nano Res. 1 (2008) 203—212.
[27] B.C. Brodie, Philos. Trans. R. Soc. Lond. 149 (1859) 249—259.
[28] K.S. Novoselov, A.K. Geim, S.V. Morozov, D. Jiang, Y. Zhang, S.V. Dubonos, I.V. Grigorieva, A.A. Firsov, Science 306 (2004) 666—669.
[29] N.A. Kotov, T. Haraszti, L. Turi, G. Zavala, R.E. Geer, I. Dekany, J.H. Fendler, J. Am. Chem. Soc. 119 (1997) 6821—6832.
[30] N.I. Kovtyukhova, P.J. Ollivier, B.R. Martin, T.E. Mallouk, S.A. Chizhik, E.V. Buzaneva, A.D. Gorchinskiy, Chem. Mater. 11 (1999) 771—778.
[31] E.R. Kleinfeld, G.S. Ferguson, Science 265 (1994) 370—373.
[32] N.A. Kotov, S. Magonov, E. Tropsha, Chem. Mater. 10 (1998) 886—895.
[33] P. Touzain, R. Yazami, J. Maire, J. Power Sources 14 (1985) 99—104.
[34] Z. Wei, D.E. Barlow, P.E. Sheehan, Nano Lett. 8 (2008) 3141—3145.
[35] J. Shen, Y. Hu, C. Li, C. Qin, M. Shi, M. Ye, Langmuir 25 (2009) 6122—6128.
[36] J. Liu, L. Tao, W. Yang, D. Li, C. Boyer, R. Wuhrer, F. Braet, T.P. Davis, Langmuir 26 (2010) 10068—10075.
[37] J. Hong, Y.S. Kang, S.W. Kang, Ind. Eng. Chem. Res. 50 (2011) 3095—3099.
[38] R.R. Nair, P. Blake, A.N. Grigorenko, K.S. Novoselov, T.J. Booth, T. Stauber, N.M.R. Peres, A.K. Geim, Science 320 (2008) 1308.
[39] D.S. Hecht, R.B. Kaner, MRS Bull. 36 (2011) 749—755.
[40] H.X. Chang, G.F. Wang, A. Yang, X.M. Tao, X.Q. Liu, Y.D. Shen, Z.J. Zheng, Adv. Funct. Mater. 20 (2010) 2893—2902.
[41] P.J. King, U. Khan, M. Lotya, S. De, J.N. Coleman, ACS Nano 4 (2010) 4238—4246.
[42] V.C. Tung, L.M. Chen, M.J. Allen, J.K. Wassei, K. Nelson, R.B. Kaner, Y. Yang, Nano Lett. 9 (2009) 1949—1955.
[43] T. Szabo, A. Szeri, I. Dekany, Carbon 43 (2005) 87—94.
[44] J. Wu, Q. Tang, H. Sun, J. Lin, H. Ao, M. Huang, Y. Huang, Langmuir 24 (2008) 4800—4805.
[45] Q. Tang, J. Wu, Q. Li, J. Lin, Polymer 49 (2008) 5329—5335.
[46] Q. Tang, Z. Tang, J. Wu, J. Lin, I. Oh, J. Mater. Chem. 21 (2011) 5378—5385.
[47] D. Chen, X. Wang, T. Liu, X. Wang, J. Li, ACS Appl. Mater. Interfaces 2 (2010) 2005—2011.
[48] D.W. Lee, T.-K. Hong, D. Kang, J. Lee, M. Heo, J.Y. Kim, B.-S. Kim, H.S. Shin, J. Mater. Chem. 21 (2011) 3438—3442.
[49] J.S. Park, S.M. Cho, W.-J. Kim, J. Park, P.J. Yoo, ACS Appl. Mater. Interfaces 3 (2011) 360—368.
[50] A. Rani, K.A. Oh, H. Koo, H.J. Lee, M. Park, Appl. Surf. Sci. 257 (2011) 4982—4989.
[51] T.-K. Hong, D.W. Lee, H.J. Choi, H.S. Shin, B.-S. Kim, ACS Nano 4 (2010) 3861—3868.
[52] S. De, J.N. Coleman, ACS Nano 4 (2010) 2713—2720.
[53] J. Zhu, B.S. Shim, M. Di Prima, N.A. Kotov, J. Am. Chem. Soc. 133 (2011) 7450—7460.
[54] B.S. Shim, J.A. Zhu, E. Jan, K. Critchley, N.A. Kotov, ACS Nano 4 (2010) 3725—3734.
[55] A. Kasry, M.A. Kuroda, G.J. Martyna, G.S. Tulevski, A.A. Bol, ACS Nano 4 (2010) 3839—3844.
[56] F. Gunes, H.-J. Shin, C. Biswas, G.H. Han, E.S. Kim, S.J. Chae, J.-Y. Choi, Y.H. Lee, ACS Nano 4 (2010) 4595—4600.
[57] S. Bae, H. Kim, Y. Lee, X.F. Xu, J.S. Park, Y. Zheng, J. Balakrishnan, T. Lei, H.R. Kim, Y.I. Song, Y.J. Kim, K.S. Kim, B. Ozyilmaz, J.H. Ahn, B.H. Hong, S. Iijima, Nat. Nanotechnol. 5 (2010) 574—578.
[58] G. Eda, G. Fanchini, M. Chhowalla, Nat. Nanotechnol. 3 (2008) 270—274.
[59] J.H. Lee, D.W. Shin, V.G. Makotchenko, A.S. Nazarov, V.E. Fedorov, Y.H. Kim, J.Y. Choi, J.M. Kim, J.B. Yoo, Adv. Mater. 21 (2009) 4383—4387.
[60] K. Jo, T. Lee, H.J. Choi, J.H. Park, D.J. Lee, D.W. Lee, B.S. Kim, Langmuir 27 (2011) 2014—2018.
[61] S.Y. Jeong, S.H. Kim, J.T. Han, H.J. Jeong, S. Yang, G.W. Lee, ACS Nano 5 (2011) 870—878.
[62] S.J. Wang, Y. Geng, Q.B. Zheng, J.K. Kim, Carbon 48 (2010) 1815—1823.
[63] G. Eda, M. Chhowalla, Adv. Mater. 22 (2010) 2392—2415.
[64] X.L. Li, X.R. Wang, L. Zhang, S.W. Lee, H.J. Dai, Science 319 (2008) 1229—1232.
[65] Y. Zhu, J.M. Tour, Nano Lett. 10 (2010) 4356—4362.
[66] H. Li, S. Pang, S. Wu, X. Feng, K. Muellen, C. Bubeck, J. Am. Chem. Soc. 133 (2011) 9423—9429.
[67] L.Y. Jiao, X.R. Wang, G. Diankov, H.L. Wang, H.J. Dai, Nat. Nanotechnol. 5 (2010) 321—325.
[68] G. Eda, M. Chhowalla, Nano Lett. 9 (2009) 814—818.
[69] S. Wang, P.J. Chia, L.L. Chua, L.H. Zhao, R.Q. Png, S. Sivaramakrishnan, M. Zhou, R.G.S. Goh, R.H. Friend, A.T.S. Wee, P.K.H. Ho, Adv. Mater. 20 (2008) 3440—3446.
[70] H. Yamaguchi, G. Eda, C. Mattevi, H. Kim, M. Chhowalla, ACS Nano 4 (2010) 524—528.
[71] J.M. Mativetsky, A. Liscio, E. Treossi, E. Orgiu, A. Zanelli, P. Samori, V. Palermo, J. Am. Chem. Soc. 133 (2011) 14320—14326.
[72] B.J. Kim, M.S. Kang, V.H. Pham, T.V. Cuong, E.J. Kim, J.S. Chung, S.H. Hur, J.H. Cho, J. Mater. Chem. 21 (2011) 13068—13073.
[73] R.Y.N. Gengler, A. Veligura, A. Enotiadis, E.K. Diamanti, D. Gournis, C. Jozsa, B.J. van Wees, P. Rudolf, Small 6 (2010) 35—39.
[74] L. Liao, J.W. Bai, Y.Q. Qu, Y.C. Lin, Y.J. Li, Y. Huang, X.F. Duan, Proc. Natl. Acad. Sci. U.S.A. 107 (2010) 6711—6715.
[75] D.B. Farmer, H.Y. Chiu, Y.M. Lin, K.A. Jenkins, F.N. Xia, P. Avouris, Nano Lett. 9 (2009) 4474—4478.
[76] K.S. Kim, Y. Zhao, H. Jang, S.Y. Lee, J.M. Kim, J.H. Ahn, P. Kim, J.Y. Choi, B.H. Hong, Nature 457 (2009) 706—710.
[77] Z.H. Liu, A.A. Bol, W. Haensch, Nano Lett. 11 (2011) 523—528.
[78] J. Kedzierski, P.L. Hsu, P. Healey, P.W. Wyatt, C.L. Keast, M. Sprinkle, C. Berger, W.A. de Heer, IEEE Trans. Electron Dev. 55 (2008) 2078—2085.
[79] S. Wang, P.K. Ang, Z.Q. Wang, A.L.L. Tang, J.T.L. Thong, K.P. Loh, Nano Lett. 10 (2010) 92—98.
[80] J.M. Tarascon, M. Armand, Nature 414 (2001) 359—367.
[81] J.R. Dahn, T. Zheng, Y.H. Liu, J.S. Xue, Science 270 (1995) 590—593.
[82] K. Sato, M. Noguchi, A. Demachi, N. Oki, M. Endo, Science 264 (1994) 556—558.
[83] A. Gerouki, M.A. Goldner, R.B. Goldner, T.E. Haas, T.Y. Liu, S. Slaven, J. Electrochem. Soc. 143 (1996) L262—L263.
[84] X. Zhao, C.M. Hayner, M.C. Kung, H.H. Kung, ACS Nano 5 (2011) 8739—8749.
[85] S.Y. Yin, Y.Y. Zhang, J.H. Kong, C.J. Zou, C.M. Li, X.H. Lu, J. Ma, F.Y.C. Boey, X.D. Chen, ACS Nano 5 (2011) 3831—3838.

[86] G.X. Wang, X.P. Shen, J. Yao, J. Park, Carbon 47 (2009) 2049—2053.
[87] D.Y. Pan, S. Wang, B. Zhao, M.H. Wu, H.J. Zhang, Y. Wang, Z. Jiao, Chem. Mater. 21 (2009) 3136—3142.
[88] P. Guo, H.H. Song, X.H. Chen, Electrochem. Commun. 11 (2009) 1320—1324.
[89] E. Yoo, J. Kim, E. Hosono, H. Zhou, T. Kudo, I. Honma, Nano Lett. 8 (2008) 2277—2282.
[90] H.B. Wang, C.J. Zhang, Z.H. Liu, L. Wang, P.X. Han, H.X. Xu, K.J. Zhang, S.M. Dong, J.H. Yao, G.L. Cui, J. Mater. Chem. 21 (2011) 5430—5434.
[91] X.F. Li, D.S. Geng, Y. Zhang, X.B. Meng, R.Y. Li, X.L. Sun, Electrochem. Commun. 13 (2011) 822—825.
[92] A.L.M. Reddy, A. Srivastava, S.R. Gowda, H. Gullapalli, M. Dubey, P.M. Ajayan, ACS Nano 4 (2010) 6337—6342.
[93] Z.S. Wu, W.C. Ren, L. Xu, F. Li, H.M. Cheng, ACS Nano 5 (2011) 5463—5471.
[94] T. Cassagneau, J.H. Fendler, Adv. Mater. 10 (1998) 877.
[95] Z.S. Wu, W.C. Ren, L. Wen, L.B. Gao, J.P. Zhao, Z.P. Chen, G.M. Zhou, F. Li, H.M. Cheng, ACS Nano 4 (2010) 3187—3194.
[96] X.J. Zhu, Y.W. Zhu, S. Murali, M.D. Stollers, R.S. Ruoff, ACS Nano 5 (2011) 3333—3338.
[97] D.H. Wang, R. Kou, D. Choi, Z.G. Yang, Z.M. Nie, J. Li, L.V. Saraf, D.H. Hu, J.G. Zhang, G.L. Graff, J. Liu, M.A. Pope, I.A. Aksay, ACS Nano 4 (2010) 1587—1595.
[98] D.H. Wang, D.W. Choi, J. Li, Z.G. Yang, Z.M. Nie, R. Kou, D.H. Hu, C.M. Wang, L.V. Saraf, J.G. Zhang, I.A. Aksay, J. Liu, ACS Nano 3 (2009) 907—914.
[99] K. Evanoff, A. Magasinski, J.B. Yang, G. Yushin, Adv. Energy Mater. 1 (2011) 495—498.
[100] S.B. Yang, X.L. Feng, S. Ivanovici, K. Mullen, Angew. Chem. Int. Ed. 49 (2010) 8408—8411.
[101] S.B. Yang, X.L. Feng, L. Wang, K. Tang, J. Maier, K. Mullen, Angew. Chem. Int. Ed. 49 (2010) 4795—4799.
[102] H.L. Wang, L.F. Cui, Y.A. Yang, H.S. Casalongue, J.T. Robinson, Y.Y. Liang, Y. Cui, H.J. Dai, J. Am. Chem. Soc. 132 (2010) 13978—13980.
[103] S.M. Paek, E. Yoo, I. Honma, Nano Lett. 9 (2009) 72—75.
[104] A.P. Yu, H.W. Park, A. Davies, D.C. Higgins, Z.W. Chen, X.C. Xiao, J. Phys. Chem. Lett. 2 (2011) 1855—1860.
[105] E. Frackowiak, F. Beguin, Carbon 39 (2001) 937—950.
[106] A.G. Pandolfo, A.F. Hollenkamp, J. Power Sources 157 (2006) 11—27.
[107] P. Simon, Y. Gogotsi, Nat. Mater. 7 (2008) 845—854.
[108] G.A. Snook, P. Kao, A.S. Best, J. Power Sources 196 (2011) 1—12.
[109] L.L. Zhang, R. Zhou, X.S. Zhao, J. Mater. Chem. 20 (2010) 5983—5992.
[110] L. Zhang, G. Shi, J. Phys. Chem. C 115 (2011) 17206—17212.
[111] A. Yu, I. Roes, A. Davies, Z. Chen, Appl. Phys. Lett. 96 (2010) 253105.
[112] T.Y. Kim, H.W. Lee, M. Stoller, D.R. Dreyer, C.W. Bielawski, R.S. Ruoff, K.S. Suh, ACS Nano 5 (2011) 436—442.
[113] L.A.L. Tang, W.C. Lee, H. Shi, E.Y.L. Wong, A. Sadovoy, S. Gorelik, J. Hobley, C.T. Lim, K.P. Loh, Small 8 (2012) 423—431.
[114] M.D. Stoller, S. Park, Y. Zhu, J. An, R.S. Ruoff, Nano Lett. 8 (2008) 3498—3502.
[115] Y. Wang, Z. Shi, Y. Huang, Y. Ma, C. Wang, M. Chen, Y. Chen, J. Phys. Chem. C 113 (2009) 13103—13107.
[116] J.J. Yoo, K. Balakrishnan, J. Huang, V. Meunier, B.G. Sumpter, A. Srivastava, M. Conway, A.L.M. Reddy, J. Yu, R. Vajtai, P.M. Ajayan, Nano Lett. 11 (2011) 1423—1427.
[117] C.X. Guo, C.M. Li, Energy Environ. Sci. 4 (2011) 4504—4507.
[118] Y. Wang, Y.P. Wu, Y. Huang, F. Zhang, X. Yang, Y.F. Ma, Y.S. Chen, J. Phys. Chem. C 115 (2011) 23192—23197.
[119] D.S. Yu, L.M. Dai, J. Phys. Chem. Lett. 1 (2010) 467—470.
[120] W.H. Shi, J.X. Zhu, D.H. Sim, Y.Y. Tay, Z.Y. Lu, X.J. Zhang, Y. Sharma, M. Srinivasan, H. Zhang, H.H. Hng, Q.Y. Yan, J. Mater. Chem. 21 (2011) 3422—3427.
[121] J. Yan, Z.J. Fan, T. Wei, W.Z. Qian, M.L. Zhang, F. Wei, Carbon 48 (2010) 3825—3833.
[122] H.L. Wang, H.S. Casalongue, Y.Y. Liang, H.J. Dai, J. Am. Chem. Soc. 132 (2010) 7472—7477.
[123] Z.S. Wu, D.W. Wang, W. Ren, J. Zhao, G. Zhou, F. Li, H.M. Cheng, Adv. Funct. Mater. 20 (2010) 3595—3602.
[124] Z. Li, J. Wang, X. Liu, S. Liu, J. Ou, S. Yang, J. Mater. Chem. 21 (2011) 3397—3403.
[125] J.T. Zhang, J.W. Jiang, X.S. Zhao, J. Phys. Chem. C 115 (2011) 6448—6454.
[126] Q. Wu, Y.X. Xu, Z.Y. Yao, A.R. Liu, G.Q. Shi, ACS Nano 4 (2010) 1963—1970.
[127] A.R. Liu, C. Li, H. Bai, G.Q. Shi, J. Phys. Chem. C 114 (2010) 22783—22789.
[128] S. Biswas, L.T. Drzal, Chem. Mater. 22 (2010) 5667—5671.
[129] L.L. Zhang, S.Y. Zhao, X.N. Tian, X.S. Zhao, Langmuir 26 (2010) 17624—17628.
[130] L. Wang, D. Wang, X.Y. Dong, Z.J. Zhang, X.F. Pei, X.J. Chen, B.A. Chen, J.A. Jin, Chem. Commun. 47 (2011) 3556—3558.
[131] X.Y. Dong, L. Wang, D. Wang, C. Li, J. Jin, Langmuir 28 (2012) 293—298.
[132] D.G. Wang, X.G. Wang, Langmuir 27 (2011) 2007—2013.
[133] H. Park, P.R. Brown, V. Buloyic, J. Kong, Nano Lett. 12 (2012) 133—140.
[134] Z.Y. Yin, S.Y. Sun, T. Salim, S.X. Wu, X.A. Huang, Q.Y. He, Y.M. Lam, H. Zhang, ACS Nano 4 (2010) 5263—5268.
[135] Y. Wang, X.H. Chen, Y.L. Zhong, F.R. Zhu, K.P. Loh, Appl. Phys. Lett. 95 (2009) 063302.
[136] J.B. Wu, H.A. Becerril, Z.N. Bao, Z.F. Liu, Y.S. Chen, P. Peumans, Appl. Phys. Lett. 92 (2008) 263302.
[137] X. Wang, L.J. Zhi, N. Tsao, Z. Tomovic, J.L. Li, K. Mullen, Angew. Chem. Int. Ed. 47 (2008) 2990—2992.
[138] X. Wang, L.J. Zhi, K. Mullen, Nano Lett. 8 (2008) 323—327.
[139] J.W.G. Wildoer, L.C. Venema, A.G. Rinzler, R.E. Smalley, C. Dekker, Nature 391 (1998) 59—62.
[140] X.C. Dong, D.L. Fu, W.J. Fang, Y.M. Shi, P. Chen, L.J. Li, Small 5 (2009) 1422—1426.
[141] Y.M. Shi, K.K. Kim, A. Reina, M. Hofmann, L.J. Li, J. Kong, ACS Nano 4 (2010) 2689—2694.
[142] H. Hibino, H. Kageshima, M. Kotsugi, F. Maeda, F.Z. Guo, Y. Watanabe, Phys. Rev. B 79 (2009).
[143] L. Kavan, J.H. Yum, M. Gratzel, ACS Nano 5 (2011) 165—172.
[144] F. Gong, H. Wang, Z.-S. Wang, Phys. Chem. Chem. Phys. 13 (2011) 17676—17682.
[145] D.W. Zhang, X.D. Li, H.B. Li, S. Chen, Z. Sun, X.J. Yin, S.M. Huang, Carbon 49 (2011) 5382—5388.
[146] J.D. Roy-Mayhew, D.J. Bozym, C. Punckt, I.A. Aksay, ACS Nano 4 (2010) 6203—6211.
[147] W.J. Hong, Y.X. Xu, G.W. Lu, C. Li, G.Q. Shi, Electrochem. Commun. 10 (2008) 1555—1558.
[148] N.L. Yang, J. Zhai, D. Wang, Y.S. Chen, L. Jiang, ACS Nano 4 (2010) 887—894.
[149] S.R. Sun, L. Gao, Y.Q. Liu, Appl. Phys. Lett. 96 (2010) 083113.
[150] M.Y. Yen, M.C. Hsiao, S.H. Liao, P.I. Liu, H.M. Tsai, C.C.M. Ma, N.W. Pu, M.D. Ger, Carbon 49 (2011) 3597—3606.
[151] Z.F. Liu, Q. Liu, Y. Huang, Y.F. Ma, S.G. Yin, X.Y. Zhang, W. Sun, Y.S. Chen, Adv. Mater. 20 (2008) 3924—3930.
[152] D.S. Yu, K. Park, M. Durstock, L.M. Dai, J. Phys. Chem. Lett. 2 (2011) 1113—1118.
[153] S.S. Li, K.H. Tu, C.C. Lin, C.W. Chen, M. Chhowalla, ACS Nano 4 (2010) 3169—3174.
[154] J.M. Yun, J.S. Yeo, J. Kim, H.G. Jeong, D.Y. Kim, Y.J. Noh, S.S. Kim, B.C. Ku, S.I. Na, Adv. Mater. 23 (2011) 4923—4928.
[155] C.X. Guo, H.B. Yang, Z.M. Sheng, Z.S. Lu, Q.L. Song, C.M. Li, Angew. Chem. Int. Ed. 49 (2010) 3014—3017.

[156] I. Robel, B.A. Bunker, P.V. Kamat, Adv. Mater. 17 (2005) 2458—2463.
[157] L. Sheeney-Haj-Khia, B. Basnar, I. Willner, Angew. Chem. Int. Ed. 44 (2005) 78—83.
[158] B. Farrow, P.V. Kamat, J. Am. Chem. Soc. 131 (2009) 11124—11131.
[159] D.M. Guldi, G.M.A. Rahman, V. Sgobba, N.A. Kotov, D. Bonifazi, M. Prato, J. Am. Chem. Soc. 128 (2006) 2315—2323.
[160] K.K. Manga, Y. Zhou, Y. Yan, K.P. Loh, Adv. Funct. Mater. 19 (2009) 3638—3643.
[161] Y.X. Liu, X.C. Dong, P. Chen, Chem. Soc. Rev. 41 (2012) 2283—2307.
[162] W.R. Yang, K.R. Ratinac, S.P. Ringer, P. Thordarson, J.J. Gooding, F. Braet, Angew. Chem. Int. Ed. 49 (2010) 2114—2138.
[163] V. Dua, S.P. Surwade, S. Ammu, S.R. Agnihotra, S. Jain, K.E. Roberts, S. Park, R.S. Ruoff, S.K. Manohar, Angew. Chem. Int. Ed. 49 (2010) 2154—2157.
[164] A. Salehi-Khojin, D. Estrada, K.Y. Lin, M.H. Bae, F. Xiong, E. Pop, R.I. Masel, Adv. Mater. 24 (2012) 53—57.
[165] J.T. Robinson, F.K. Perkins, E.S. Snow, Z.Q. Wei, P.E. Sheehan, Nano Lett. 8 (2008) 3137—3140.
[166] F. Schedin, A.K. Geim, S.V. Morozov, E.W. Hill, P. Blake, M.I. Katsnelson, K.S. Novoselov, Nat. Mater. 6 (2007) 652—655.
[167] Y.P. Dan, Y. Lu, N.J. Kybert, Z.T. Luo, A.T.C. Johnson, Nano Lett. 9 (2009) 1472—1475.
[168] J.D. Fowler, M.J. Allen, V.C. Tung, Y. Yang, R.B. Kaner, B.H. Weiller, ACS Nano 3 (2009) 301—306.
[169] Q. Ji, I. Honma, S.-M. Paek, M. Akada, J.P. Hill, A. Vinu, K. Ariga, Angew. Chem. Int. Ed. 49 (2010) 9737—9739.
[170] C. Zhu, S. Guo, Y. Zhai, S. Dong, Langmuir 26 (2010) 7614—7618.
[171] Y. Mao, Y. Bao, W. Wang, Z. Li, F. Li, L. Niu, Talanta 85 (2011) 2106—2112.
[172] Y. Cui, B. Zhang, B. Liu, H. Chen, G. Chen, D. Tang, Microchim. Acta 174 (2011) 137—144.
[173] H.F. Xu, H. Dai, G.N. Chen, Talanta 81 (2010) 334—338.
[174] Q.O. Zeng, J.S. Cheng, L.H. Tang, X.F. Liu, Y.Z. Liu, J.H. Li, J.H. Jiang, Adv. Funct. Mater. 20 (2010) 3366—3372.
[175] S.J. Guo, D. Wen, Y.M. Zhai, S.J. Dong, E.K. Wang, ACS Nano 4 (2010) 3959—3968.
[176] L.Y. Cao, Y.L. Liu, B.H. Zhang, L.H. Lu, ACS Appl. Mater. Interfaces 2 (2010) 2339—2346.
[177] G. Zeng, Y. Xing, J. Gao, Z. Wang, X. Zhang, Langmuir 26 (2010) 15022—15026.
[178] H. Wu, J. Wang, X.H. Kang, C.M. Wang, D.H. Wang, J. Liu, I.A. Aksay, Y.H. Lin, Talanta 80 (2009) 403—406.
[179] X. Wang, J. Wang, H. Cheng, P. Yu, J. Ye, L. Mao, Langmuir 27 (2011) 11180—11186.
[180] X.C. Li, H.J. Zhou, P. Yu, L. Su, T. Ohsaka, L.Q. Mao, Electrochem. Commun. 10 (2008) 851—854.
[181] N. Mohanty, V. Berry, Nano Lett. 8 (2008) 4469—4476.
[182] Y. Ohno, K. Maehashi, K. Matsumoto, J. Am. Chem. Soc. 132 (2010) 18012—18013.
[183] X.C. Dong, Y.M. Shi, W. Huang, P. Chen, L.J. Li, Adv. Mater. 22 (2010) 1649—1653.
[184] M. Zhou, Y.M. Zhai, S.J. Dong, Anal. Chem. 81 (2009) 5603—5613.
[185] L.Y. Feng, Y. Chen, J.S. Ren, X.G. Qu, Biomaterials 32 (2011) 2930—2937.
[186] L.Y. Feng, L. Wu, J.S. Wang, J.S. Ren, D. Miyoshi, N. Sugimoto, X.G. Qu, Adv. Mater. 24 (2012) 125—131.
[187] S.J. He, B. Song, D. Li, C.F. Zhu, W.P. Qi, Y.Q. Wen, L.H. Wang, S.P. Song, H.P. Fang, C.H. Fan, Adv. Funct. Mater. 20 (2010) 453—459.
[188] H.X. Chang, L.H. Tang, Y. Wang, J.H. Jiang, J.H. Li, Anal. Chem. 82 (2010) 2341—2346.
[189] B. Zhang, T. Cui, Appl. Phys. Lett. 98 (2011).
[190] M.H. Yang, A. Javadi, H. Li, S.Q. Gong, Biosens. Bioelectron. 26 (2010) 560—565.
[191] M. Yue, J.C. Stachowiak, H. Lin, R. Datar, R. Cote, A. Majumdar, Nano Lett. 8 (2008) 520—524.
[192] J.M. Nam, C.S. Thaxton, C.A. Mirkin, Science 301 (2003) 1884—1886.
[193] X. Yu, B. Munge, V. Patel, G. Jensen, A. Bhirde, J.D. Gong, S.N. Kim, J. Gillespie, J.S. Gutkind, F. Papadimitrakopoulos, J.F. Rusling, J. Am. Chem. Soc. 128 (2006) 11199—11205.
[194] G.F. Zheng, F. Patolsky, Y. Cui, W.U. Wang, C.M. Lieber, Nat. Biotechnol. 23 (2005) 1294—1301.
[195] X. Zhang, S. Li, X. Jin, S. Zhang, Chem. Commun. 47 (2011) 4929—4931.
[196] M.A. Rafiee, W. Lu, A.V. Thomas, A. Zandiatashbar, J. Rafiee, J.M. Tour, N.A. Koratkar, ACS Nano 4 (2010) 7415—7420.
[197] M.K. Shin, B. Lee, S.H. Kim, J.A. Lee, G.M. Spinks, S. Gambhir, G.G. Wallace, M.E. Kozlov, R.H. Baughman, S.J. Kim, Nat. Commun. 3 (2012).
[198] J.W. Suk, R.D. Piner, J.H. An, R.S. Ruoff, ACS Nano 4 (2010) 6557—6564.
[199] C. Gomez-Navarro, M. Burghard, K. Kern, Nano Lett. 8 (2008) 2045—2049.
[200] J. Liang, Y. Huang, L. Zhang, Y. Wang, Y. Ma, T. Guo, Y. Chen, Adv. Funct. Mater. 19 (2009) 2297—2302.
[201] P. Laaksonen, A. Walther, J.M. Malho, M. Kainlauri, O. Ikkala, M.B. Linder, Angew. Chem. Int. Ed. 50 (2011) 8688—8691.
[202] J.M. Malho, P. Laaksonen, A. Walther, O. Ikkala, M.B. Linder, Biomacromolecules 13 (2012) 1093—1099.
[203] X. Yang, Y. Tu, L. Li, S. Shang, X.-m. Tao, ACS Appl. Mater. Interfaces 2 (2010) 1707—1713.
[204] U. Khan, P. May, A. O'Neill, J.N. Coleman, Carbon 48 (2010) 4035—4041.
[205] Z. Xu, C. Gao, Macromolecules 43 (2010) 6716—6723.
[206] L. Nguyen Dang, U. Hippi, J.T. Korhonen, A.J. Soininen, J. Ruokolainen, L.-S. Johansson, J.-D. Nam, L.H. Sinh, J. Seppala, Polymer 52 (2011) 5237—5242.
[207] M.A. Rafiee, J. Rafiee, Z. Wang, H.H. Song, Z.Z. Yu, N. Koratkar, ACS Nano 3 (2009) 3884—3890.
[208] K. Wakabayashi, P.J. Brunner, J.i. Masuda, S.A. Hewlett, J.M. Torkelson, Polymer 51 (2010) 5525—5531.
[209] H. Kim, S. Kobayashi, M.A. AbdurRahim, M.L.J. Zhang, A. Khusainova, M.A. Hillmyer, A.A. Abdala, C.W. Macosko, Polymer 52 (2011) 1837—1846.
[210] J.R. Potts, D.R. Dreyer, C.W. Bielawski, R.S. Ruoff, Polymer 52 (2011) 5—25.
[211] T. Kuilla, S. Bhadra, D.H. Yao, N.H. Kim, S. Bose, J.H. Lee, Prog. Polym. Sci. 35 (2010) 1350—1375.
[212] H. Kim, A.A. Abdala, C.W. Macosko, Macromolecules 43 (2010) 6515—6530.
[213] X. Zhao, Q.H. Zhang, Y.P. Hao, Y.Z. Li, Y. Fang, D.J. Chen, Macromolecules 43 (2010) 9411—9416.
[214] B. Das, K.E. Prasad, U. Ramamurty, C.N.R. Rao, Nanotechnology 20 (2009).
[215] X. Zhao, Q.H. Zhang, D.J. Chen, P. Lu, Macromolecules 43 (2010) 2357—2363.
[216] X.M. Yang, L.A. Li, S.M. Shang, X.M. Tao, Polymer 51 (2010) 3431—3435.
[217] Z.H. Tang, Y.D. Lei, B.C. Guo, L.Q. Zhang, D.M. Jia, Polymer 53 (2012) 673—680.
[218] R.K. Layek, S. Samanta, A.K. Nandi, Carbon 50 (2012) 815—827.
[219] Y.X. Xu, W.J. Hong, H. Bai, C. Li, G.Q. Shi, Carbon 47 (2009) 3538—3543.
[220] O.C. Compton, S.W. Cranford, K.W. Putz, Z. An, L.C. Brinson, M.J. Buehler, S.T. Nguyen, ACS Nano 6 (2012) 2008—2019.
[221] N.V. Medhekar, A. Ramasubramaniam, R.S. Ruoff, V.B. Shenoy, ACS Nano 4 (2010) 2300—2306.

[222] D.D. Kulkarni, I. Choi, S. Singamaneni, V.V. Tsukruk, ACS Nano 4 (2010) 4667—4676.
[223] P. Podsiadlo, A.K. Kaushik, E.M. Arruda, A.M. Waas, B.S. Shim, J.D. Xu, H. Nandivada, B.G. Pumplin, J. Lahann, A. Ramamoorthy, N.A. Kotov, Science 318 (2007) 80—83.
[224] V.A. Sinani, D.S. Koktysh, B.G. Yun, R.L. Matts, T.C. Pappas, M. Motamedi, S.N. Thomas, N.A. Kotov, Nano Lett. 3 (2003) 1177—1182.
[225] A.A. Mamedov, A. Belov, M. Giersig, N.N. Mamedova, N.A. Kotov, J. Am. Chem. Soc. 123 (2001) 7738—7739.
[226] D. Gross, A.S. Susha, T.A. Klar, E. Da Como, A.L. Rogach, J. Feldmann, Nano Lett. 8 (2008) 1482—1485.
[227] B.I. MacDonald, A. Martucci, S. Rubanov, S.E. Watkins, P. Mulvaney, J.J. Jasieniak, ACS Nano 6 (2012) 5995—6004.
[228] M. Yang, K.Q. Cao, L. Sui, Y. Qi, J. Zhu, A. Waas, E.M. Arruda, J. Kieffer, M.D. Thouless, N.A. Kotov, ACS Nano 5 (2011) 6945—6954.
[229] H. Zhang, J. Shih, J. Zhu, N.A. Kotov, Nano Lett. 12 (2012) 3391—3398.
[230] Y. Bai, S. Ho, N.A. Kotov, Nanoscale 4 (2012) 4393—4398.
[231] C.M. Andres, I. Larraza, T. Corrales, N.A. Kotov, Adv. Mater. (2012), http://dx.doi.org/10.1002/adma.201201378.

Ming Yang received his B.S. degree in chemistry from Jilin University, PR China in 2003. He then completed his Ph.D. degree in 2008 from Department of Chemistry at Jilin University, under the guidance of Professor Shouhua Feng. He is currently a postdoctoral fellow in Professor Nicholas A. Kotov's group at the University of Michigan. His research interests include self-organization of nanocolloids, nanoscale drug delivery, nanoplasmonics and polymer nanocomposite thin films.

Ying Hou received her B.S. degree (2003) and Ph.D. degree (2008) both in chemistry from Jilin University, PR China. She is a research scientist in Nico Technologies Corp at Ann Arbor. Her research interests include ultra-strong nanocomposites and self-cleaning surfaces.

Nicholas A. Kotov is a Joseph B. and Florence V. Professor of Engineering at the University of Michigan. He is working on the preparation and utilization of advanced composites made by the layer-by-layer assembly and other nanostructured thin films. Prof. Kotov's work is devoted to nanoscale design of ultrastrong materials for military/civilian application and to self-organization of nanoscale particles into complex systems. He is particularly interested in biomimetic aspects of composites, nanoparticle-protein analogy, and nanoscale chiral systems. His publications include 230+ papers devoted to the mechanical, electrical properties of nanocomposites, self-organized nanoscale processes, and optoelectronic materials. He is serving as an Associate Editor for ACS Nano, and as a member of Advisory Board of nanotechnology journals such as Chemistry of Materials, Advanced Functional Materials, and Langmuir. He was awarded 2012 AICHE Stine Award for research in self-organized structures at nanoscale and 2012 Kennedy Family Award for the research in nanocomposites. He also received NSF CAREER award, Junior Faculty Award for Scholarly Excellence, Humboldt Fellowship (Germany), CNRS Fellowship (France), Walton Award (Ireland), and Welliver Award (Boeing).